Turbulent pair dispersion of inertial particles

By J. BEC[1], L. BIFERALE[2], A. S. LANOTTE[3], A. SCAGLIARINI[2] and F. TOSCHI[4]

[1] Université de Nice-Sophia Antipolis, CNRS, Observatoire de la Côte d'Azur, Laboratoire Cassiopée, Bd. de l'Observatoire, 06300 Nice, France

[2] Department of Physics and INFN, University of Rome Tor Vergata, Via della Ricerca Scientifica 1, 00133 Roma, Italy

[3] ISAC-CNR, Istituto di Scienze dell'Atmosfera e del Clima, Via Fosso del Cavaliere 100, 00133 Roma and INFN, Sezione di Lecce, 73100 Lecce Italy

[4] Department of Physics and Department of Mathematics and Computer Science, Eindhoven University of Technology, 5600 MB Eindhoven, The Netherlands and Istituto per le Applicazioni del Calcolo CNR, Viale del Policlinico 137, 00161 Roma, Italy

(Received 15 April 2009)

The relative dispersion of pairs of inertial particles in incompressible, homogeneous, and isotropic turbulence is studied by means of direct numerical simulations at two values of the Taylor-scale Reynolds number $Re_\lambda \sim 200$ and $Re_\lambda \sim 400$, corresponding to resolutions of 512^3 and 2048^3 grid points, respectively. The evolution of both heavy and light particle pairs is analysed at varying the particle Stokes number and the fluid-to-particle density ratio. For particles much heavier than the fluid, the range of available Stokes numbers is $St \in [0.1:70]$, while for light particles the Stokes numbers span the range $St \in [0.1:3]$ and the density ratio is varied up to the limit of vanishing particle density. For heavy particles, it is found that turbulent dispersion is schematically governed by two temporal regimes. The first is dominated by the presence, at large Stokes numbers, of small-scale caustics in the particle velocity statistics, and it lasts until heavy particle velocities have relaxed towards the underlying flow velocities. At such large scales, a second regime starts where heavy particles separate as tracers particles would do. As a consequence, at increasing inertia, a larger transient stage is observed, and the Richardson diffusion of simple tracers is recovered only at large times and large scales. These features also arise from a statistical closure of the equation of motion for heavy particle separation that is proposed, and which is supported by the numerical results.
In the case of light particles with high density ratios, strong small-scale clustering leads to a considerable fraction of pairs that do not separate at all, although the mean separation increases with time. This effect strongly alters the shape of the probability density function of light particle separations.

1. Introduction

Suspensions of dust, droplets, bubbles, and other finite-size particles advected by incompressible turbulent flows are commonly encountered in many natural phenomena (see, e.g., Csanady 1980, Eaton & Fessler 1994, Falkovich *et al.*. 2002, Post & Abraham 2002, Shaw 2003, Toschi & Bodenschatz 2009). Understanding their statistical properties is thus of primary importance. From a theoretical point of view, the problem is more complicated than in the case of fluid tracers, i.e. point-like particles with the same density as

the carrier fluid. Indeed, when the suspended particles have a finite size and a density ratio different from that of the fluid, they have inertia and do not follow exactly the flow. As a consequence, correlations between particle positions and structures of the underlying flow appear. It is for instance well known that heavy particles are expelled from vortical structures, while light particles tend to concentrate in their cores. This results in the formation of strong inhomogeneities in the particle spatial distribution, an effect often refered to as *preferential concentration* (see Douady *et al.* 1991, Squires & Eaton 1991, Eaton & Fessler 1994). This phenomenon has gathered much attention, as it is revealed by the amount of recently published theoretical work (Balkovsky *et al.* 2001, Zaichik *et al.* 2003, Falkovich & Pumir 2004), and numerical studies (Collins & Keswani 2004, Chun *et al.* 2005, Bec *et al.* 2007, Goto & Vassilicos 2008). Progresses in the statistical characterization of particle aggregates have been achieved by studying particles evolving in stochastic flows by Sigurgeirsson & Stuart 2002, Mehlig & Wilkinson 2004, Bec *et al.* 2005, Olla 2002 and in two-dimensional turbulent flows by Boffetta *et al.* 2004. Also, single trajectory statistics have been addressed both numerically and experimentally for small heavy particles (see, e.g., Bec *et al.* 2006, Cencini *et al.* 2006, Gylfason *et al.* 2006, Gerashchenko *et al.* 2008, Zaichik & Alipchenkov 2008, Ayyalasomayajula *et al.* 2008, Volk *et al.* 2008), and for large particles (Qureshi *et al.* 2007, Xu & Bodenschatz 2008). The reader is refered to Toschi & Bodenschatz 2009 for a review.

In this paper we are concerned with particle pair dispersion, that is with the statistics, as a function of time, of the separation distance $\boldsymbol{R}(t) = \boldsymbol{X}_1(t) - \boldsymbol{X}_2(t)$ between two inertial particles, labelled by the subscripts 1 and 2 (see Bec *et al.* 2008, Fouxon & Horvai 2008, Derevich 2008 for recent studies on that problem). In homogeneous turbulence, it is sufficient to consider the statistics of the instantaneous separation of the positions of the two particles. These are organised in different families according to the values of their Stokes number St, and of their density mismatch with the fluid, β.

For our purposes, the motion of particle pairs, with given (St, β) values and with initial separations inside a given spherical shell, $R = |\boldsymbol{X}_1(t_0) - \boldsymbol{X}_2(t_0)| \in [R_0, R_0 + dR_0]$ is followed until particle separation reaches the large scale of the flow. With respect to the case of simple tracers, the time evolution of the inertial particle pair separation $R(t)$ becomes a function not only of the initial distance R_0, and of the Reynolds number of the flow, but also of the inertia parameters (St, β).

A key question that naturally arises is how to choose the initial spatial and velocity distributions of inertial pairs. Indeed, it is known that heavy (resp. light) particles tend to concentrate preferentially in hyperbolic (resp. elliptic) regions of the advecting flow, with spatial correlation effects that may extend up to the inertial range of scales, as shown in Bec *et al.* 2007. Moreover, when inertia is high enough, the particle pair velocity difference, $\delta_R V = |\boldsymbol{V}_1(\boldsymbol{X}_1(t), t) - \boldsymbol{V}_2(\boldsymbol{X}_2(t), t)|$, may not go smoothly to zero when the particle separations decreases, a phenomenon connected to the formation of *caustics*, see Wilkinson & Mehlig 2005, Falkovich & Pumir 2007. In our numerical simulations, particles of different inertia are injected into the flow and let evolve until they reach a stationary statistics for both spatial and velocity distributions. Only after this transient time, pairs of particles with fixed intial separation are selected and then followed in the spatial domain to study relative dispersion.

By reason of the previous considerations, the main issue is to understand the role played by the spatial inhomogeneities of the inertial particle concentration field and by the presence of caustics on the pair separations, at changing the degree of inertia. We remark that these two effects can be treated as independent only in the limit of very small and very large inertia. In the former case, particles tend to behave like tracers and move with the underlying fluid velocity: preferential concentration may affect only their

separation. In the opposite limit, particles distribute almost homogeneously in the flow: however, due to their ballistic motion, they can reach nearby positions with very different velocities (Falkovich *et al.*. 2002). In any other case of intermediate inertia, both these effects are present and may play a role in the statistics of inertial pair separation.

It is worth anticipating the two main results of this study:
(i) The separation between heavy particles can be described in terms of two time regimes: a first regime is dominated by inertia effects, and considerable deviations from the tracers case arise in the inertial relative dispersion; in the second one, the tracers behaviour is recovered since inertia is weak and appears only in subdominant corrections that vanish as $1/t$. The crossover between these two regimes defines a new characteristic spatial and temporal scale, connected to both the *size of caustics* and the Stokes number, which influences the particle separation for not too long time-lags and not too large scale.
(ii) The strong clustering properties that are typical of light particles may lead to the fact that many pairs do not separate at all: their statistical weight is clear in the separation probability density function (PDF), which develops a well defined power-law left tail.

It would clearly be also interesting to investigate the dependence upon the Reynolds number of the inertial particle pair separation. Small-scale clustering seems to be poorly dependent on the degree of turbulence of the carrier flow (Collins & Keswani 2004, Bec *et al.* 2007), while much less is known about the Reynolds number dependence of the caustics statistics. Our numerical data do not allow to explore this question in detail, so that we will restrict ourselves to show data associated to the two Reynolds numbers in all cases when differences are not significative.

In the case of fluid tracers, the standard observables are the time evolutions of the mean square separation and of the separation probability density function, for which well established predictions exist since the pioneering work of Richardson 1929. We contrast these observables obtained for tracers with the results for heavy and light inertial particles.

The paper is organised as follows. In §2, we briefly recall the basic equations of motion and describe the numerical simulations. In §3, we analyse the stationary distribution of heavy particle velocity differences, conditioned on the particle initial separation, highlighting both the presence of small-scale caustics and the effects of particle inertia at those scales corresponding to the inertial range of turbulence. In §4 we study the behaviour of the mean separation distance of heavy pairs, at changing the Stokes number St; we also analyse the influence of the caustics in the initial statistics on the subsequent pair separation evolution. A *mean-field* model, which is able to capture the main numerical findings, is proposed in the same section. The time evolution of the separation probability density functions is discussed in §5 and we present the data for light particles in §6. In §7 we summarise the main findings.

2. Equation of motion and numerical details

We present results from direct numerical simulations of turbulent flows seeded with inertial particles. The flow phase is described by the Navier-Stokes equations for the velocity field $\boldsymbol{u}(\boldsymbol{x}, t)$

$$\partial_t \boldsymbol{u} + \boldsymbol{u} \cdot \nabla \boldsymbol{u} = -\nabla p + \nu \nabla^2 \boldsymbol{u} + \boldsymbol{f}, \quad \nabla \cdot \boldsymbol{u} = 0\,. \tag{2.1}$$

The statistically homogeneous and isotropic external forcing $\boldsymbol{f}$ injects energy in the first low wave number shells, by keeping constant their spectral content (see Chen *et al.* 1993). The kinematic viscosity ν is chosen such that the Kolmogorov length scale $\eta \approx \delta x$, where δx is the grid spacing: this choice ensures a good resolution of the small-scale velocity

	N	Re_λ	η	δx	ε	ν	τ_η	$t_{\rm dump}$	δt
Run I	512	185	0.01	0.012	0.9	0.002	0.047	0.004	0.0004
Run II	2048	400	0.0026	0.003	0.88	0.00035	0.02	0.00115	0.000115

TABLE 1. Eulerian parametres for the two runs analysed here: Run I and Run II in the text. N is the number of grid points in each spatial direction; Re_λ is the Taylor-scale Reynolds number; η is the Kolmogorov dissipative scale; $\delta x = \mathcal{L}/N$ is the grid spacing, with $\mathcal{L} = 2\pi$ denoting the physical size of the numerical domain; $\tau_\eta = \sqrt{\nu/\varepsilon}$ is the Kolmogorov dissipative time scale; ε is the kinetic energy dissipation; ν is the kinematic viscosity; $\tau_{\rm dump}$ is the time interval between two successive dumps along particle trajectories; δt is the time step.

dynamics. The numerical domain is cubic and 2π-periodic in the three directions of space. We use a fully dealiased pseudospectral algorithm with $2^{\rm nd}$ order Adam-Bashforth time-stepping (for details see Bec *et al.* 2006, Cencini *et al.* 2006). We performed two series of DNS: Run I with numerical resolution of 512^3 grid points, and the Reynolds number at the Taylor scale $Re_\lambda \approx 200$; Run II with 2048^3 resolution and $Re_\lambda \approx 400$. Details of the runs can be found in Table 1.

The particle phase is constituted by millions of heavy and light particles — the latter only for Run I — with different intrinsic characteristics. Particles are assumed to be with size much smaller than the Kolmogorov scale of the flow, η, and with a negligible Reynolds number relative to the particle size. In this limit, the equations ruling their dynamics take the particularly simple form:

$$\dot{\boldsymbol{X}} = \boldsymbol{V} \,, \qquad \dot{\boldsymbol{V}} = -\frac{1}{\tau_s}\left[\boldsymbol{V} - \boldsymbol{u}(\boldsymbol{X},t)\right] + \beta\, D_t\boldsymbol{u}(\boldsymbol{X},t) \,, \tag{2.2}$$

where the dots denote time derivatives. The particle position and velocity are $(\boldsymbol{X}(t), \boldsymbol{V}(t))$, respectively; $\boldsymbol{u}(\boldsymbol{X}(t),t)$ is the Eulerian fluid velocity evaluated at the particle position, and $D_t\boldsymbol{u}$ is the so-called added mass term, which measures the fluid acceleration along particle trajectory. The adimensional constant $\beta = 3\rho_f/(\rho_f + 2\rho_p)$ accounts for the added mass effect through the density contrast between particles ρ_p and fluid ρ_f. The particle response time, appearing in the Stokes drag, is $\tau_s = 2\rho_p a^2/(9\rho_f\nu)$, where a is the particle radius. Particle inertia is quantified by the *Stokes number* that is defined as $St = \tau_s/\tau_\eta$, where $\tau_\eta = (\nu/\varepsilon)^{1/2}$ is the flow Kolmogorov timescale and ε the average rate of energy injection. Equation (2.2) has been derived in Maxey & Riley 1983 under the assumption of very dilute suspensions, where particle-particle interactions (collisions) and hydrodynamic coupling to the flow can be neglected.

For Run I, we show results for the following set of (St, β) families: (i) very heavy particles $[\beta = 0]$: $St = 0.0, 0.6, 1.0, 3.3$; (ii) light particles $[\beta = 2, 3]$: $St = 0.3, 1.2, 4.1$. For each family the typical number of particle pairs that are followed is around 5×10^4. For Run II, we show results only for heavy particles but with a larger range of variation in the Stokes number: $St = 0.0, 0.6, 1.0, 3.0, 10, 30, 70$. Typical number of particle pairs for each family is $\sim 10^4$. Once injected particles have relaxed to their steady-state statistics, pairs have been selected with the following initial separations: $R_0 \le \eta$ and $R_0 \in [4:6]\eta$ for both Run I and Run II, and $R_0 \in [9:11]\eta$ for Run II only.

Beside the time evolution of particle pairs, we also have instantaneous snapshots of the two phases (fluid and dispersed), with a much higher particle statistics: around 10^6 per family for Run I, and 10^8 per family for Run II. These are used to measure the stationary — i.e. not along the trajectories — distribution of particle velocity increments discussed in next section.

3. Stationary distributions: velocity increments conditioned on particles separation

Turbulent pair dispersion for tracers is classically based on the application of similarity theory for Eulerian velocity statistics: depending on the value of space and time scales, velocity increment statistics differently affect the way tracers separate. This results in different regimes for relative dispersion, see e.g. Sawford 2001.

In the case of inertial particles, the same reasoning holds, so that to analyse the way inertial pairs separate in time, the stationary statistics of particles velocity differences has to be investigated first. A stationary distribution for the typical velocity differences between two inertial particles is obtained by imposing periodic boundary conditions inside the physical volume and then measuring velocities on such a thermalised configuration.

We are interested in the scaling behaviour of velocity increments at varying the degree of inertia and the distance between the particles (in the dissipative or inertial range of the turbulent fluid flow). To fix the notation, we denote by U_0 the typical large-scale velocity of the fluid tracers and by L the integral scale of the flow. Moreover we define

$$\delta_R V_{St} \;=\; |\boldsymbol{V}_1(\boldsymbol{X}_1(t)) - \boldsymbol{V}_2(\boldsymbol{X}_2(t))|, \tag{3.1}$$

as the velocity difference at scale R, conditioned on the presence of a pair of particles with Stokes number St, separated with a distance $R = |\boldsymbol{X}_1(t_0) - \boldsymbol{X}_2(t_0)|$. Since we are here interested in the case of heavy particles only, the Stokes number is sufficient to identify a given particle family. For convenience, we introduce a specific notation for the tracer stationary velocity statistics: $\delta_R u \;=\; \delta_R V_{(St=0)}$, which is exactly equal to the Eulerian velocity increment at scale R.

Recently, Bec *et al.* 2008 have shown that to describe inertial pair dispersion in synthetic flows it is useful to introduce the local or *scale-dependent* Stokes number, using the ratio between the particle response time and the typical eddy turnover time $\tau_R = R/\delta_R u$ of the underlying fluid at a given scale: $St(R) = \tau_s/\tau_R \sim \tau_s \delta_R u/R$. For real turbulent flow where different scaling ranges are present, we can equivalently define a scale dependent Stokes number $St(R)$ that recovers the usual definition of the Stokes number $St(R) \simeq St = \tau_s/\tau_\eta$ when $R \ll \eta$ and behaves as $St(R) \sim \tau_s \varepsilon^{1/3} R^{-2/3}$ when $R \gg \eta$. The typical behaviour of $St(R)$ is sketched in Fig. 1, for two different values of the Stokes number $St = 3, 70$ and using a Batchelor-like parametrisation of the fluid velocity (see Meneveau 1996):

$$\delta_R u \;=\; U_0 \frac{R}{(\eta^2 + R^2)^{1/3}}. \tag{3.2}$$

For Stokes numbers, St, order unity or larger, there always exists a typical scale where the local Stokes number, $St(R)$, becomes order unity,

$$R^*(St) = \eta\, St^{3/2}. \tag{3.3}$$

Such a scale, which is well in the inertial range if the Stokes number St is sufficiently large, can be considered a rough estimate of the upper bound for the region of scales where inertia plays an important role in the particle dynamics. We expect that two main features might be important in characterising the inertial particle stationary velocity statistics $\delta_R V$, with respect to that of tracers $\delta_R u$. The first concerns the small-scale behaviour of the particle velocity statistics. At small scales $R \ll \eta$ and for large-enough Stokes numbers, the presence of caustics makes the particle velocity increments not differentiable.

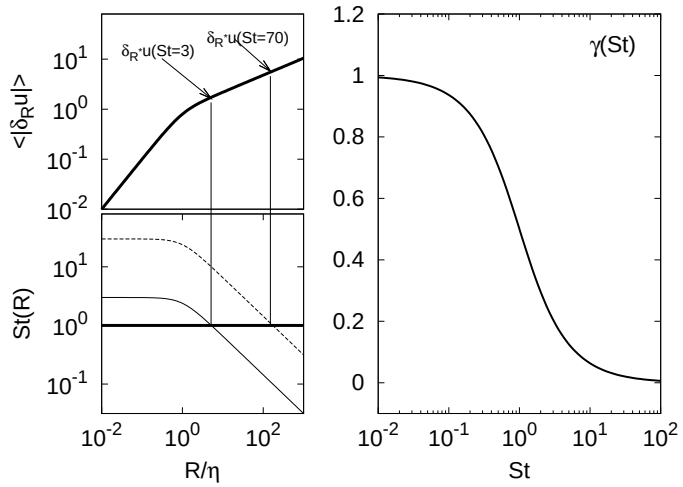

FIGURE 1. Left panels. Bottom figure: behaviour of the scale-dependent Stokes number, $St(R)$ as a function of the scale R normalised with the Kolmogorov scale η, for two Stokes numbers $St = 3, 70$ (bottom and top, respectively). The horizontal thick line is for $St(R) = 1$. Top figure: the scaling behaviour for the fluid tracer velocity increments versus the scale as given by (3.2). Notice that the scales R^* where $St(R^*) = 1$ fall in the inertial range of the Eulerian fluid velocity. Right panel: the function $\gamma(St)$ defining the small scales power law behaviour of caustics statistics at changing inertia. Notice that for small values of the Stokes number St, $\gamma \to 1$, i.e. particle velocity is differentiable; at high inertia, $\gamma \to 0$ indicating the existence of discontinuities in the particle velocity increment statistics.

This feature can be accounted for by saying that

$$\delta_R V_{St} \sim V_{St}^{\eta} \left(\frac{R}{\eta}\right)^{\gamma(St)} ; \qquad R \ll \eta, \tag{3.4}$$

where the V_{St}^{η} is a constant prefactor and the function $\gamma(St)$ gives the typical scaling of caustic-like velocity increments. Indeed we do expect that at changing the inertia of the particles, the statistical weight of caustics might monotonically vary as follows: at small St, $\lim_{St\to 0} \gamma(St) = 1$, i.e. the value for smooth, differentiable Eulerian statistics of tracers; at large values $St \to \infty$, it should approach the discontinuous limit $\gamma(St) \to 0$, valid for particles that do not feel underlying fluid fluctuations at all. The right panel of Fig. 1 shows the typical shape of the function $\gamma(St)$ that is expected to be valid for turbulent flows.

The second important feature concerns the particle velocity statistics at scales larger than the scale $R^*(St)$ previously defined, but smaller than the integral scale of the fluid flow. For any fixed Stokes number and for a large-enough Reynolds number, we expect that inertia becomes weaker and weaker, by going to larger and larger scales $R \gg R^*(St)$. In such a case, particle velocity increments are expected to approach the underlying fluid velocity increments:

$$\delta_R V_{St} \to V_{St}^0 \, \delta_R u \sim V_{St}^0 \, U_0 \left(\frac{R}{L}\right)^{1/3} ; \qquad R^*(St) \ll R \ll L, \tag{3.5}$$

where for simplicity we have neglected possible intermittent correction to the Kolmogorov 1941 (K41) scaling of the fluid velocity (see Frisch 1995 for details). Clearly, the Reynolds number has to be sufficiently large to provide a well-developed scaling region $R^*(St) \ll R \ll L$, before approaching the large scale L. We emphasise that in (3.5), an adimensional

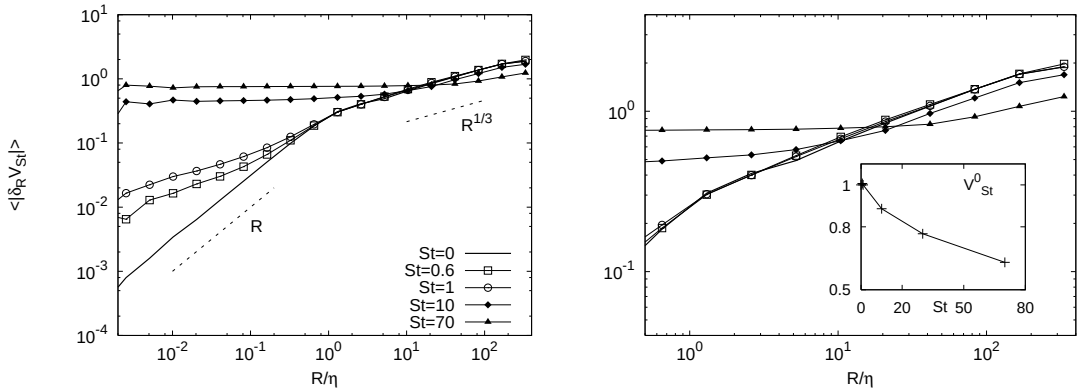

FIGURE 2. Right figure: particle velocity structure function of order $p = 1$ versus the scale R/η, for various Stokes numbers, $St = 0, 0.6, 1, 10, 70$, and for Reynolds number $Re_\lambda \sim 400$, Run II. The statistics for fluid tracers ($St = 0$) correspond to the solid line. Statistical errors are of the order of twice the size of symbols for scales smaller then η and become comparable with the size of symbols in the inertial range of fluid velocity statistics. The differentiable scaling behaviour $\propto R$ in the dissipative range, and the Kolmogorov 1941 behaviour $\propto R^{1/3}$ in the inertial range of scales are also shown. Left figure: zoom-in of the inertial range, same symbols as right. Inset: behaviour of the amplitude prefactor, V^0_{St} as a function of the Stokes number St, as measured from the velocity increments at the integral scale L, Run II.

normalisation factor V^0_{St} has been introduced: it takes into account possible filtering effects induced by inertia at large scales. The normalisation is such that $V^0_{(St=0)} = 1$, while for any Stokes larger than zero $V^0_{(St)} \leq 1$.

In Fig. 2 we test the validity of the previous picture by analyzing the typical velocity fluctuation, $\langle|\delta_R V_{St}|\rangle$, at changing Stokes number and for data of Run II at Reynolds number $Re_\lambda \sim 400$. At small scales one detect the presence of caustics in the velocity statistics, with a non smooth scaling behaviour below the Kolmogorov scale η. At scales within the inertial range and when the Stokes number is sufficiently large, the effect of caustics affects also particle velocity statistics, up to a characteristic scale which becomes larger and larger by increasing particle inertia. Beyond this scale, particle velocity increments tend to approach the scaling behaviour of the fluid tracers, but their amplitude is depleted of a factor $1/V^0_{St}$, which increases with the Stokes number, as shown in the inset of the right-hand panel of Fig. 2. A similar behaviour is expected for higher order fluctuations, if we neglect the role of intermittency.

It is interesting to consider the scaling behaviour of particle velocity in terms of the underlying velocity statistics, not only at very small or very large separations, but for any value of the scale R. This is not straigthforward, since we have to account not only of the fluid Eulerian statistics at the dissipative and inertial range of scales, but also the modifications due to the inertia. This is responsible, as we have seen, for the appeareance of a new relevant scale, and for filtering effects in the velocity amplitude.

To fully characterise particle velocity increments, we notice that the Stokes scale, $R^*(St)$ defines a typical *Stokes-velocity*: this is the fluid velocity increment at the Stokes scale, $\delta u^*(St) \sim \delta_{R^*} u$ (see left panel of Fig. 1). Previous reasonings can be summarised in the following interpolation formula for the heavy particle velocity increment:

$$\delta_R V_{St} \;=\; V^0_{St}\,(\delta_R u)^{\gamma(St(R))}\,\left[(\delta_R u)^2 + c_1\,(\delta u^*(St))^2\right]^{[1-\gamma(St(R))]/2}\,. \qquad (3.6)$$

The above expression is a Batchelor-like parametrisation but in the velocity space, with a transient velocity given by the Stokes velocity, $\delta u^*(St)$.

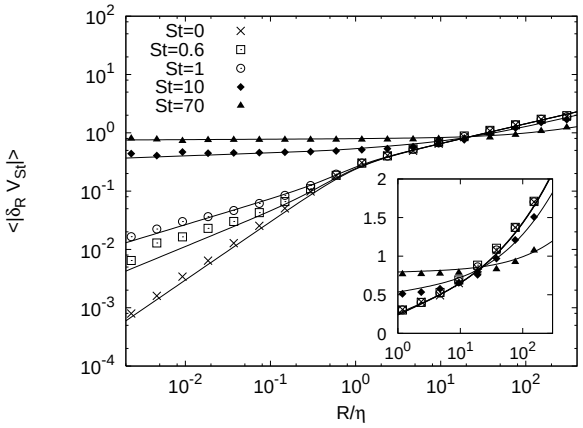

FIGURE 3. Scaling behaviour of the particle velocity structure function of order one, versus the normalised scale R/η. Solid lines: fit of the data of Fig. 2, Run II, using the interpolation formula (3.6). Here the large scale prefactors V_{St}^0 are those measured on Run II of the simulation, and shown in the inset of the right panel of Fig. 2. Inset: enlargement of the crossover range, where $\delta_R u \sim \delta_R V$.

Once known the large scale normalization function V_{St}^0, the caustic exponent $\gamma(x)$ (introduced in Bec *et al.* 2005) and the reference fluid velocity increment $\delta_R u$, then the formula has one free parameter only. It is the prefactor c_1 appearing in front of the Stokes velocity $\delta u^*(St)$, whose value depends again on the inertia of the particles.

In Fig. 3, we show the result of the fit in terms of the expression (3.6), where the caustics scaling exponent has been chosen as $\gamma(x) = [1 - 2/\pi \, \mathrm{atan}(x)]$: this functional form provides a good fit to the numerical results. Details of the small-scale caustic statistics will be reported elsewhere.

The qualitative trend is very well captured by the interpolation function proposed. Notice that in (3.6), the argument of $\gamma(St)$ is not the simple Stokes number at the Kolmogorov scale, but the scale-dependent one $St(R)$: $\gamma(St) \to \gamma(St(R))$. This further ingredient is needed to take into account the fact that in presence of a rough underlying fluid velocity, as it happens in the inertial range of scales, no simple power law behaviour is expected for the scaling of particle velocity statistics. This was previously remarked in Bec *et al.* 2008, in the study of heavy particle turbulent dispersion in random flows.

Equation (3.6) clearly matches the two limiting behaviours for very small and very large separations. In the former case, inertia dominates the small-scale velocity statistics with respect to the underlying smooth fluid velocity, and caustics lead to a pure power-law behaviour,

$$\delta_R V \sim (\delta_R u)^{\gamma(St)} \sim V_{St}^0 \left(\frac{R}{L}\right)^{\gamma(St)} ; \qquad R \ll \eta, \tag{3.7}$$

where the local Stokes number has attained its dissipative limit $St(R) \to St$.

In the latter case, at very large scales $R \gg R^*(St)$ inertia is subleading, and the typical velocity difference between particles is close to the fluid velocity increment,

$$\delta_R V_{St} \sim V_{St}^0 \, \delta_R u; \qquad \eta \ll R^*(St) \ll R. \tag{3.8}$$

At intermediate scales, for large Stokes, $St \geq 1$, inertia brings a non-trivial dependency via the scale-dependent Stokes number, $St(R)$, and we expect a pseudo power-law scaling:

$$\delta_R V_{St} \sim (\delta_R u)^{\gamma(St(R))} \sim R^{\gamma(St(R))/3}; \qquad \eta \ll R \ll R^*(St) \, . \tag{3.9}$$

Summarising, we propose that at changing the Stokes and Reynolds numbers, different

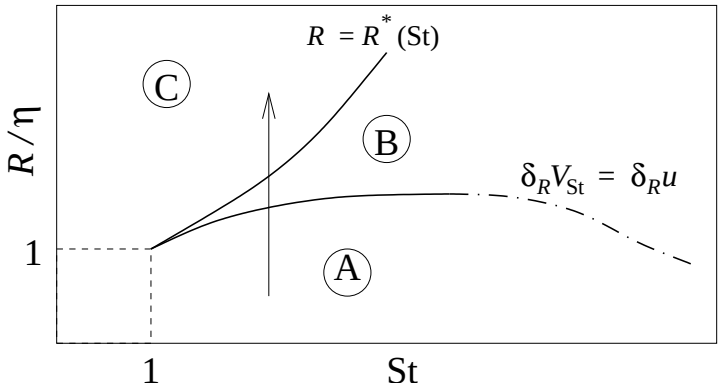

FIGURE 4. Sketch of the different regimes expected in the parameter space of inertia, St, and scale separation R. The curve $St(R^*) = 1$ separate the region of low inertia $St(R) \leq 1$, region (C), from the regions where inertia is important $St(R) \geq 1$, regions (A) and (B). Further we can distinguish the separation regime where inertia is important and particle velocity difference larger than the fluid one at the same scale, region (A), from the intermediate regime where inertia is still important particle velocity difference is smaller that the corresponding fluid one, region (B). Separation between region (A) and (B) is given by the curve $\delta_R V_{St} = \delta_R u$. For relative dispersion of pairs of Stokes St starting at a given separation R, one typically starts from the corresponding position in this plane and then evolve upwards along the vertical arrow.

regimes governing the particle velocity statistics can be distinguished. The relevance of such regimes of the particle velocity statistics for the associate relative dispersion dynamics can be easily explained with the help of the sketch reported in Fig. 4. In the parameter space of inertia and scale separation (St, R), we can distinguish three regions depending whether inertia is strong or weak, and whether particle velocity difference is large or not with respect of the fluid velocity difference at comparable scale. In agreement with what commented before, we pose that the curve $St(R^*) = 1$ distinguishes the region of weak $(St(R) \leq 1)$ and strong inertia $(St(R) \geq 1)$.

Regime (A) is such that inertia is important since the scale $R^*(St) \gg \eta$, and moreover the typical particle velocity increments are larger than the fluid increments. In the region (B), inertia is still important but particle velocity increments are depleted with respect to the fluid increments. This typically happens for large Stokes numbers, and in our DNS is visible only for very large separations $R(t)$ of the highest Stokes $St = 70$. Finally, regime (C) is characterised by a weak inertia, which appears only in the filtering factor for the velocity large-scale amplitude and possibly in sub-leading corrections to the tracers relative dispersion.

Even for the largest value of the Reynolds and Stokes numbers achieved in our DNS, it is very difficult to disentangle quantitatively the above mentioned regimes, because of the closeness of the three relevant scales, η, $R^*(St)$, and L. Still, the quality of the fit shown in Fig. 3 using the global functional dependence given by Eqn. (3.6) makes us confident that the main physical features are correctly captured. Before closing this section, we note that there is no reason to assume that the functional form entering in the pseudo-power law scaling in the inertial range, $\gamma(St(R))$, in (3.9) is equal the one characterizing the scaling in the viscous range, $\gamma(St)$, in Eqn. (3.7). Hint for this observation come from results obtained in Bec *et al.* 2008 for random flows, where a very high statistical accuracy can be achieved: there, depending if the underlying fluid velocity is spatially smooth or rough, a slightly different functional form has been found.

The previous analysis gives us a clear quantitative picture of the scale and velocity ranges where caustics play a role in the particle dynamics. For example, for moderate

Stokes numbers, we have important departure from the tracers statistics only for very small scales, i.e. caustics gives a singular contributions to the particle velocity increments inside the viscous range; then, at larger scales, the particle velocity scaling become indistinguishable from the tracer velocities. Clearly, for such Stokes, no important corrections for particle separation evolution is expected with respect to the usual Richardson dispersion observed for tracers. This is because particle pairs tends to separate, and very soon all pairs will attain separations where their velocities are very close to the underlying fluid. On the other hand, for very heavy particles, those with Stokes time falling inside the inertial range of fluid velocity statistics, the contribution from the caustics will be felt also at relatively large scales, up to $R \sim R^*(St)$. Pair separations attain such scales when the initially large relative velocity difference has relaxed and become smaller than the corresponding fluid one — crossing from region (A) to (B). Notice that at $R \sim R^*(St)$, we have that $\delta_{R^*} V_{St} \simeq V^0_{St} \delta_{R^*} u$, i.e. there is a non-trivial effect from inertia. Moreover, for large Stokes, at scales $R > R^*(St)$, particle velocity increments are smaller than the fluid counterparts, indicating an important depletion induced by the Stokes drag on the particle evolution.

It is clear from the above discussion that new physics should appear for the value of inertia and scales separation of region (B). This regime — that we can not access with the present data — is the one where a new law of pair separation should appear as recently suggested by Fouxon & Horvai 2008. A discussion of the dispersion regimes of inertial particle pairs follows in the next section in terms of the time behaviour of the mean square separation distance.

4. Dispersion regimes and corrections due to inertia

In this section we analyse the effects of inertia on the mean square separation of heavy particle pairs with a given initial separation distance, R_0 at time $t = t_0$, as a function of the Stokes number:

$$\langle (R(t))^2 \,|\, R_0, t_0 \rangle_{St} \;=\; \langle |\boldsymbol{X}_1(t) - \boldsymbol{X}_2(t)|^2 \rangle_{St}, \tag{4.1}$$

where in the left-hand side the average is performed over all pairs of particles such that $|\boldsymbol{X}_1(t_0) - \boldsymbol{X}_2(t_0)| = R_0$. The study of the relative dispersion of small, neutrally buoyant tracer particles has recently been the subject of renewed interest. This has been motivated by the fact that very accurate — highly resolved in time and space — data have become available, experimentally (Ott & Mann 2000, Bourgoin *et al.* 2006) and numerically (Yeung & Borgas 2004, Biferale *et al.* 2005, Biferale *et al.* 2006). These studies have confirmed what was known since the works of Richardson 1929 and Batchelor 1952, i.e. the existence of different dispersive regimes for tracer pairs in turbulent flows, depending on the value of their initial distance and on the time scale considered.

When released in a statistically homogeneous and isotropic, turbulent flow with an initial separation R_0 in the inertial range for fluid velocity, i.e. $\eta \simeq R_0 \ll L$, tracer pairs initially separate according so the so-called Batchelor regime,

$$\langle (R(t))^2 | R_0, t_0 \rangle_{St=0} \simeq R_0^2 + C(\varepsilon R_0)^{2/3}\, t^2; \qquad \tau_\eta \ll (t - t_0) \ll t_B\,, \tag{4.2}$$

where C is supposed to be a universal constant, and ε is the average kinetic energy dissipation of the flow. This *ballistic* regime appears because initially tracers separate *as if* the underlying velocity field were frozen, and it lasts for a time scale that is a function of the initial separation itself, $t_B = \left(R_0^2/\varepsilon\right)^{1/3}$ (see Batchelor 1952, Bourgoin *et al.* 2006). After such a transient initial time, the relative separation dynamics forgets the initial

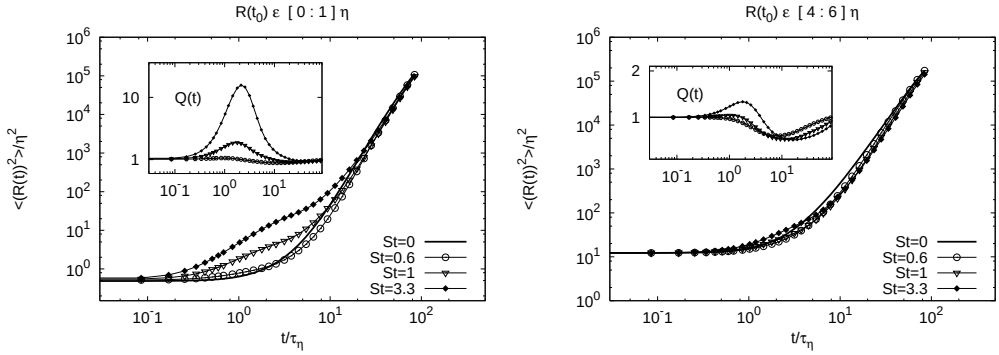

FIGURE 5. Mean square separation versus time, for heavy particles at changing St and the initial distance R_0. Time is normalised with the Kolmogorov time scale τ_η. Left panel: $St = 0, 0.6, 1,$ and 3.3; initial distance $R_0 \in [0:1]\eta$, Run I. Error bars due to statistical fluctuations are of the order of the symbol size. Notice that the two largest Stokes numbers show a time lag interval where separation proceeds faster than tracers. Inset: ratio between the heavy particle separation and the tracer data, $Q(t)$ versus time, for $St = 0.6, 1,$ and 3.3. Same symbols as in the body of the figure are used. Right panel: mean square separation versus time, but with a larger initial distance, $R_0 \in [4:6]\eta$. Stokes numbers are the same as in the left panel. Notice that now only the dispersion of particle pairs with $St = 3.3$ exhibits a small departure from the underlying fluid, as shown by the $Q(t)$ indicator in the inset. For the smaller Stokes, typical size of caustics is smaller than the initial separation R_0, and particle pairs therefore separate as fluid tracers do.

conditions and tracers separate explosively with a power law behaviour given by the Richardson law:

$$\langle (R(t))^2 | R_0, t_0 \rangle_{(St=0)} \sim g\, t^3; \qquad t_B \ll (t - t_0) \ll T_L\,, \tag{4.3}$$

where g is known as the Richardson constant. As set out in Monin & Yaglom Monin & Yaglom 2007, the tracer separation PDF — that will be discussed later — has a similar scaling behaviour in these ranges.

A remarkable fact of the Richardson dispersion (4.3) is the disappearance of the dependence on the initial separation R_0, an effect also dubbed *intrinsic stochasticity* (E & Vanden Eijnden 2000), which is just the signature of the non-Lipschitz nature of the velocity field driving the separation between tracers, when their mutual distance is in the inertial range of fluid velocity statistics. The experimental and numerical validation of the previous prediction (4.3) has proved to be particularly difficult, the main reason being the strong contamination from viscous and large scale effects in the tracers dynamics. To overcome these problems, a series of techniques have been developed, including the study of *doubling time statistics*; i.e. the probability distribution function of the time needed for a pair to double its separation (Boffetta & Sokolov 2002, Biferale *et al.* 2005). Thanks to these techniques, a fairly good agreement on the value of the Richardson constant has been achieved. Here, we want to study how the tracer behaviour is modified by the presence of small-scale caustics in particular and by inertia effects in general, for the case of heavy particle pairs. Standard direct measurements of the moments of separation as a function of time will be considered, while application of doubling time statistics is left for future studies.

In Fig. 5, we show the behaviour for the mean square separation at varying the Stokes number, and for two values of the initial separation. We start with data at the lowest resolution, i.e. Run I at $Re_\lambda \simeq 200$, and for moderate Stokes numbers, $St \sim \mathcal{O}(1)$. Initial distances are chosen equal to $R_0 \leq \eta$ (left panel) and $R_0 \in [4{:}6]\,\eta$ (right panel).

If the initial distance is small enough (left panel), the presence of caustics in the particle

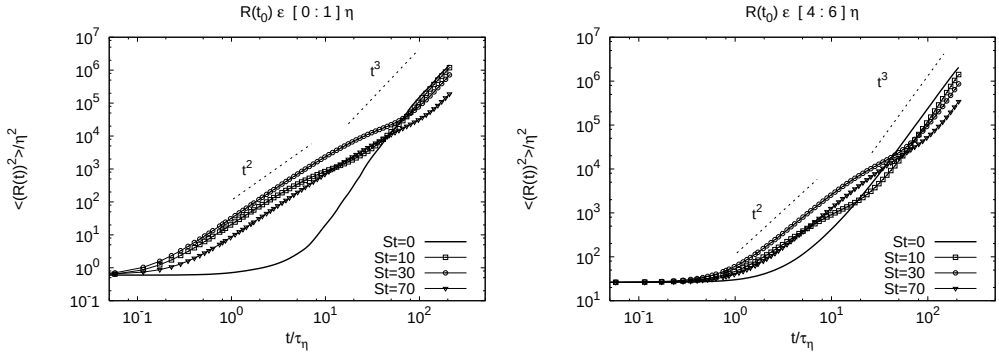

FIGURE 6. Mean square separations versus time, for pairs with $St = 10, 30, 70$, at $Re_\lambda = 400$. Left and right panels refer to the two initial distance $R_0 \in [0\!:\!1]\eta$ and $R_0 \in [4\!:\!6]\eta$, respectively. Error bars due to statistical fluctuations are of the order of the symbols size. Tracers (solid lines) are also shown for comparison. Notice the ballistic behaviour for the heavy particle separation observed in the *caustics dominated* time interval. For very large time-lags a Richardson-like behaviour starts to develop but with a less intense overall speed of separation, due to the depletion effects of the $V_{St}^{(0)}$ prefactor in the particle velocity increments for large Stokes numbers. The slopes of the Batchelor, $\langle R^2(t)\rangle \propto t^2$, and Richardson, $\langle R^2(t)\rangle \propto t^3$ dispersion regimes are also drawn for reference.

velocity field at initial time gives a very remarkable departure from the tracer behaviour. At increasing the Stokes number, such departure is more and more evident, and it lasts for a time lag which becomes longer and longer. For the highest value of the Stokes number shown in the left panel of Fig. 5 ($St = 3.3$), a sensible difference from the tracer behaviour is observed over almost two decades: $t \in [0.1\!:\!10]\,\tau_\eta$. A way to better visualise the departure from the tracer statistics consists in plotting the mean square separation for heavy pairs of different Stokes numbers, normalised to the tracer one, that is

$$Q(t) \;=\; \frac{\langle (R(t))^2 \rangle_{St}}{\langle (R(t))^2 \rangle_{(St=0)}}. \tag{4.4}$$

This quantity is shown in the insets of Figure 5. For heavy pairs starting at $R_0 \simeq \eta$ and with $St = 3.3$, the relative difference is as large as 10 at its maximum for $t \sim \tau_\eta$. However, such effect becomes progressively less important if we start the separation experiment from larger initial distances as shown in the right panel of the same figure. This is because, at these same Stokes numbers, the deviation of particle velocity difference with respect to the underlying fluid, due to caustics, has already decreased. This is equivalent to state that, for these Stokes numbers, the typical size of caustics is smaller than the initial separation R_0, and particle pairs therefore separate as fluid tracers do. At larger time lags, whatever the value of the initial separation, the Richardson dispersion regime is recovered.

We now consider what happens for larger Stokes numbers. In Fig. 6, we show the results for the mean square separation of $St = 10, 30$, and 70 and for the large Reynolds number, $Re_\lambda \simeq 400$. Both initial distances, $R_0 \in [0\!:\!1]\eta$ and $R_0 \in [4\!:\!6]\eta$ are displayed. As one can see, for the large value of $St = 70$, the tracer-like behaviour is never recovered, and even the separation of pairs starting with the largest distance R_0 is affected. The transient regime dominated by the caustics invades the whole inertial range: since particle pairs need a very long time to decrease their initial velocity difference to the value of the fluid increment at the corresponding scale, they separate with a quasi-ballistic behaviour:$\langle R^2(t)\rangle_{St} \propto t^2$.

The above scenario can be interpreted in terms of caustic-*dimensions*. At any value of the

inertia, there exist a spatial length, of the order of the scale $R^*(St)$, which identifies the typical spatial size of caustics, i.e. the range of scales where particle velocity increments are uncorrelated from the underlying fluid velocity field. If the initial pair separation R_0 is taken inside this region (left panel of Fig. 5), particle pair separation starts much faster than for fluid tracers, because of the much more intense velocity differences felt by the pairs inside the caustics. When particle pairs reach a separation larger than $R^*(t)$, they start to be synchronised with the underlying fluid velocity, recovering the typical Richardson dispersion. However, if the initial separation is larger than the caustics size, the evolution of inertial particle pairs is almost indistinguishable from the tracers. Finally, whether or not a Richardson-like behaviour is recovered for very large inertia, may depend on the Reynolds number also. In the limit of larger and larger Reynolds, at fixed Stokes number, one may expect a final recovery of the fluid tracers behaviour even for very heavy particle pairs.

4.1. *Mean-field approach to heavy particle dispersion*

The turbulent relative dispersion of fluid tracers can be easily modelled by applying K41 scaling theory to the fluid velocity increments governing particle separation dynamics (see, e.g., Ouellette *et al.* 2006). Indeed, if $\boldsymbol{R}(t)$ is the tracer separation vector at a given time, its evolution is completely specified by the equation

$$\dot{\boldsymbol{R}}(t) \,=\, \boldsymbol{u}(\boldsymbol{X}_1,t) - \boldsymbol{u}(\boldsymbol{X}_2,t) \,=\, \delta_R\boldsymbol{u}(\boldsymbol{R},t)\,, \tag{4.5}$$

together with the initial condition $\boldsymbol{R}(t_0)=\boldsymbol{R}_0$. Hence, we can directly write an equation for the root-mean-square separation $r(t) \,\equiv\, \langle|\boldsymbol{R}(t)|^2 \,|\, R_0,t_0\rangle^{1/2}$

$$\dot{r} = \frac{1}{r}\,\langle \boldsymbol{R}(t)\cdot\delta_R\boldsymbol{u}(\boldsymbol{R}(t),t)\,|\,R_0,t_0\rangle\,, \quad \text{with } r(t_0)=R_0. \tag{4.6}$$

We next assume the following mean-field closure for the right-hand side:

$$\langle \boldsymbol{R}(t)\cdot\delta_R\boldsymbol{u}(\boldsymbol{R}(t),t)\,|\,R_0,t_0\rangle \approx \langle \boldsymbol{R}^2\,|\,R_0,t_0\rangle^{1/2}\,\langle\hat{\boldsymbol{R}}\cdot\delta_R\boldsymbol{u}\rangle \,=\, r\,S_1^{/\!/\!/}(r), \tag{4.7}$$

where $S_1^{/\!/\!/}(r)$ is the first-order Eulerian longitudinal structure function of the underlying homogeneous and isotropic turbulent flow. According to K41 phenomenology, this structure function behaves in the inertial range as $S_1^{/\!/\!/}(r) \simeq C\,\varepsilon^{1/3}r^{1/3}$, where C is an order-unity constant. This closure finally leads to

$$\dot{r} = C\,\varepsilon^{1/3}r^{1/3}, \quad \text{so that} \quad r(t) = \Big[R_0^{2/3} + (2C/3)\,\varepsilon^{1/3}(t-t_0)\Big]^{3/2}. \tag{4.8}$$

Such an approximation gives a complete qualitative picture of the time evolution of the mean square separation between tracers. In particular, it encompasses the two important regimes of relative dispersion: when $(t-t_0) \ll t_B = (3/2C)\,\varepsilon^{-1/3}R_0^{2/3}$, a Taylor expansion of the solution (4.8) gives the Batchelor regime $r(t) \simeq R_0 + C\,(\varepsilon R_0)^{1/3}\,(t-t_0)$, while when $(t-t_0) \gg t_B$, one recovers Richardson's law $r(t) \simeq (2C/3)^{3/2}\varepsilon^{1/2}\,t^{3/2}$.

In the case of inertial particles, the number of degrees of freedom to describe the dynamics is obviously increased: the separation between two heavy particles obeys

$$\ddot{\boldsymbol{R}}(t) \,=\, -\frac{1}{\tau_s}\Big[\dot{\boldsymbol{R}}(t) - \delta_R\boldsymbol{u}(\boldsymbol{R},t)\Big]\,. \tag{4.9}$$

In order to derive *mean-field* equations one has to track simultaneously the average distance and velocity difference between particles. For this we follow the same spirit as for tracers and introduce the particle velocity structure function $v(t) \,\equiv\, \langle|\delta_R\boldsymbol{V}(t)|^2\,|\,R_0,t_0\rangle^{1/2}$, where $\delta_R\boldsymbol{V}(t) \,=\, \dot{\boldsymbol{R}}(t)$ is the velocity difference between the two particles. One can pro-

ceed as previously to write from (4.9) exact equations for $r(t)$ and $v(t)$:

$$\ddot{r} \,=\, \frac{1}{r}(v^2-\dot{r}^2) - \frac{1}{\tau_s}\left[\dot{r} - \frac{1}{r}\,\langle \boldsymbol{R}\cdot\delta_R\boldsymbol{u}\rangle\right], \tag{4.10}$$

$$\dot{v} \,=\, -\frac{1}{\tau_s}\left[v - \frac{1}{v}\,\langle \delta_R\boldsymbol{V}\cdot\delta_R\boldsymbol{u}\rangle\right], \tag{4.11}$$

where for the sake of a lighter notation the indication of conditional ensemble averages was dropped. It is worth noticing that the root-mean-square velocity difference $v(t)$ evolves with a dynamics that resembles closely that of heavy particles. However, $v(t)$ does not coincide with the time derivative of the mean distance $r(t)$. It is thus useful to rewrite the above equations introducing a sort of transverse particle velocity component w defined as

$$\dot{r} \,=\, v - w\,. \tag{4.12}$$

We can write an exact equation also for the evolution of w

$$\dot{w} \,=\, -\frac{1}{\tau_s}w - (2v-w)\frac{w}{r} - \frac{1}{\tau_s}\left[\frac{1}{r}\langle \boldsymbol{R}\cdot\delta_R\boldsymbol{u}\rangle - \frac{1}{v}\langle \delta_R\boldsymbol{V}\cdot\delta_R\boldsymbol{u}\rangle\right]. \tag{4.13}$$

Of course, equations (4.11), (4.12), and (4.13) are not closed without supplying the correlation between the particle evolution and the underlying fluid. As in the case of tracers, the first unclosed term appearing in the right-hand side of (4.13) is approximated by (4.7). The next unclosed term involving the correlation between fluid and particle velocity differences is approximated by

$$\langle \delta_R\boldsymbol{V}\cdot\delta_R\boldsymbol{u}\rangle \approx \langle|\delta_R\boldsymbol{V}|^2\rangle^{1/2}\,\langle|\delta_R\boldsymbol{u}|^2\rangle^{1/2} \,=\, v\,S_2^{1/2}(r)\,, \tag{4.14}$$

where $S_2(r)$ denotes the full second-order structure function of the fluid velocity field. When r is in the inertial range, K41 phenomenology implies that $S_2(r)\propto(\varepsilon r)^{2/3}$. Finally these approximations lead to a closed set of equations for the time evolution of the average separation and velocities r, v, and w

$$\dot{r} \,=\, v - w\,, \tag{4.15}$$

$$\dot{v} \,=\, \frac{1}{\tau_s}[C\,\varepsilon^{1/3}r^{1/3} - v]\,, \tag{4.16}$$

$$\dot{w} \,=\, -\frac{1}{\tau_s}w - (2v-w)\,\frac{w}{r} + \frac{1}{\tau_s}B\,\varepsilon^{1/3}r^{1/3}\,, \tag{4.17}$$

where B and C are positive order-unity dimensionless constants, reflecting the lack of control on the prefactors of the scaling laws in the closures (4.7) and (4.14). This system of equations is supplemented by the initial conditions $r(t_0)=R_0$, $v(t_0)=\langle|\delta_{R_0}\boldsymbol{V}|^2\rangle^{1/2}$ and $w(t_0)=v(t_0)-\langle\boldsymbol{R}_0\cdot\delta_{R_0}\boldsymbol{V}\rangle/R_0$, which clearly depend on the dispersion experiment under consideration. It is worth noticing that this system of equations reduces to the mean-field equation (4.8) for tracers in the limit of vanishing inertia $\tau_s\to 0$.

Similarly to the case of tracers, the crude approximation (4.15)-(4.17) of the evolution of the root-mean-square distance between heavy inertial particles is able to capture the main features of the separation time behaviour. In Fig. 7, we show the result of the numerical integration of the set of equation (4.15)-(4.17) obtained by an appropriate choice of the free parameters (see figure caption), together with DNS data from Run II, for two different large values of the Stokes number. For fixed initial separation and at increasing the intensity of the caustics velocity increments in the initial condition (i.e. at increasing inertia), the transient deviation from the Richardson behaviour become more and more evident at intermediate times (of the order of the Stokes time τ_s, not shown).

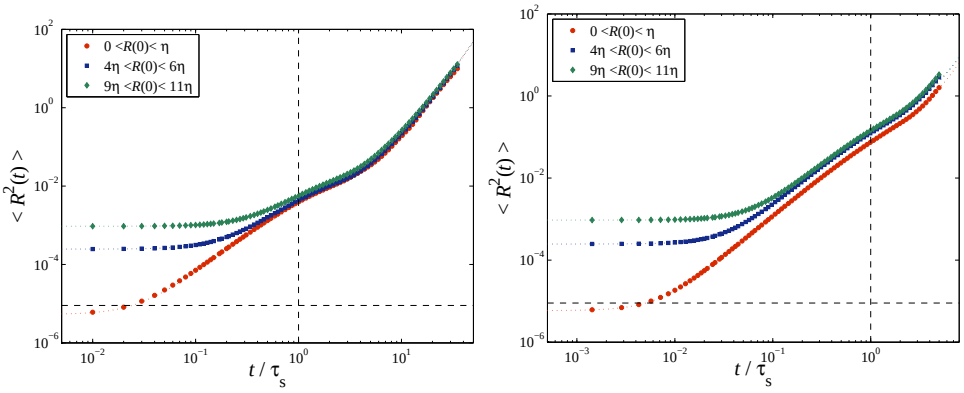

FIGURE 7. Mean square separation versus time, for Run II and Stokes numbers $St = 10$ (left panel) and $St = 70$ (right panel). Data are shown for the available choices of the initial separations : $R_0 \leq \eta$, $R_0 \in [4:6]\,\eta$, and $R_0 \in [9:11]\,\eta$ (from bottom to top). Symbols stand for DNS data, while solid lines are mean-field solutions. Adimensional prefactors are $B = 0$ and $C \simeq 2$. Notice that time is made adimensional with the Stokes time τ_s. Vertical dashed lines mark $t/\tau_s = 1$.

Clearly such a simple approach can be valid only in a limited region of the phase space, where the initial conditions are, at least, at the edge of the inertial range so that K41 scaling is correct for the fluid velocity second-order increments. Moreover, the matching scale where particle velocity increments become of the order of the fluid increments has to fall in the inertial range too: if this is not the case, then pairs enter the regime where inertia is important but particle relative velocity is small at scales of the dissipative range, and the mean-field closure proposed above becomes inadequate. A detailed quantitative comparison of the realm of applicability of the mean-field approach — including effects of viscous scales and small-scale caustics — will be the object of future work.

4.2. *Cross-over between relaxation to the fluid velocity and Richardson behaviour*

Despite its simplicity, the mean-field approach described above is able to correctly reproduce the pair dispersion of heavy particles with initial data in the inertial range. We might wonder if one can draw an even simpler qualitative picture of pair dispersion. For this, we consider the behaviour of particle pairs with moderately large Stokes numbers, for which inertia plays an important role for the initial transient and the Richardson behaviour is slowly recovered well inside the inertial range of scales. For simplicity, we assume that the scale where the fluid and particle velocity becomes of the same order, $\delta_R \boldsymbol{V} \sim \delta_R \boldsymbol{u}$, and the scale $R^*(St)$, where inertia ceases to be important, are very close. As it is clear from the sketch of Fig. 4, this may not be always the case because of the effect of the normalisation factor V^0_{St} for large Stokes: in the picture, it corresponds to Stokes number with a narrow transient region (B).

The general picture then goes as follows. Initially particles separate almost ballistically during a time which is of the order of (or larger than) the time needed by their initial, caustics-dominated, velocities to relax to the fluid velocity. After that time, particles behave as tracers and reconcile with a standard Richardson dispersion. This is a first order approximation since (*i*) the fluid flow actually correlates to the particle dynamics already at very small times, and (*ii*) inertia effects are present up to large times as previously discussed. Nevertheless, such an approximation should give the two correct qualitative asymptotic behaviours, at small and large time scales. Since we consider moderately large values of the Stokes number, the initial typical particle velocity can

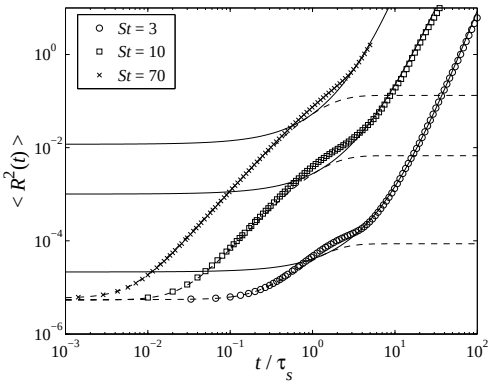

FIGURE 8. Mean square separation versus time from DNS data of Run II, for three different values of the Stokes numbers. Notice that time is normalised with the Stokes time τ_s. Solid lines represent the initial, almost ballistic evolution due to the exponential relaxation of velocity statistics, and the dashed lines correspond to the Richardson regime. With a suitable tuning of the free parameters, here the Richardson constant g and the initial velocity increment value $\langle(\delta_R V(t_0))^2\rangle$, both temporal behaviours are reproduced.

be assumed to be much larger than the fluid velocity, i.e. $|\delta_R \boldsymbol{V}| \gg |\delta_R \boldsymbol{u}|$. Under these hypotheses, there is an initial time interval during which difference between particle velocities obeys $\delta_R \dot{\boldsymbol{V}} \approx -(\delta_R \boldsymbol{V})/\tau_s$ [see (4.11)], and thus $\delta_R \boldsymbol{V}(t) \simeq (\delta_R \boldsymbol{V}(t_0))\, e^{-(t-t_0)/\tau_s}$. As a consequence, the mean square separation between particles evolves initially as:

$$\langle |\boldsymbol{R}^2(t)| \,|\, R_0, t_0\rangle = R_0^2 + 2\tau_s \langle \boldsymbol{R}(t_0)\cdot\delta_R\boldsymbol{V}(t_0)\rangle (1-e^{-(t-t_0)/\tau_s}) + \tau_s^2 \langle (\delta_R \boldsymbol{V}(t_0))^2\rangle (1-e^{-(t-t_0)/\tau_s})^2. \tag{4.18}$$

This should be approximately valid up to a time scale, in the inertial range, where $|\delta_R \boldsymbol{V}| \sim |\delta_R \boldsymbol{u}| \sim (\varepsilon R)^{1/3}$: it is easy to show that such a time scale is proportional to the particle response time τ_s. For larger times, inertia effects become subdominant and heavy pair dispersion suddenly gets synchronised to a Richardson like regime. Nevertheless, this Richardson regime has started only after the previous relaxation has ended, that is at a distance much larger than the original separation R_0 of the particle pair. The combination of this initial exponential relaxation of heavy particles with moderately large inertia, plus the later standard Richardson diffusion are the two main features due to inertia in the inertial pair dispersion. This is indeed confirmed by Figure (8), where we compare DNS data for mean square separation, with the two phenomenological regimes just described, for which we have assumed that $\langle \boldsymbol{R}\cdot\delta_R\boldsymbol{V}(t_0)\rangle \simeq 0$. As we can see, the main qualitative trends of the small and large time behaviours are very well captured.

4.3. *Subleading terms in the Richardson regime*

We have seen in previous subsections that the most noticeable effect of inertia on the mean pair dispersion is a long transient regime that takes place before reaching a Richardson explosive separation (4.3), and that this regime is due to the relaxation of particle velocities to those of the fluid. As we now argue, at larger times — corresponding to regime (C) — there is still an effect of particle inertia that can be measured in terms of subleading corrections to the Richardson law. To estimate these corrections, let us assume that in the mean-field equation (4.16), the term stemming from the fluid velocity $C\varepsilon^{1/3} r^{1/3}$ is much larger than the inertia term $\tau_s \dot{v}$. This is true when $St(r) \ll 1$, i.e. at times t when $r(t) \gg R^*(St)$. In this asymptotic, one can infer that the transverse velocity component w is much smaller than the total velocity v, so that $\dot{r} \simeq v$ (see eq. (4.12)). In

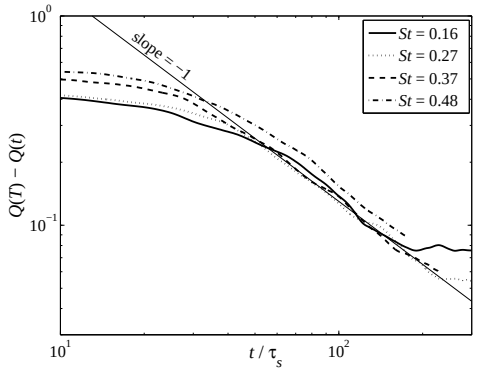

FIGURE 9. Large-time behaviour of the mean square separation normalised to that of tracers as defined from Eqn. (4.4) for Run I and various values of the Stokes number as labeled. Deviations from the fluid tracer Richardson law behave as $(t/\tau_s)^{-1}$. The limiting value $Q(T)$ has been chosen different from unity as effects of inertia are still present at the largest scale of the flow.

the spirit of the weak inertia expansion derived in Maxey 1987, we next write a Taylor expansion of (4.16) to obtain

$$\dot{r} \approx v \approx C\varepsilon^{1/3} r^{1/3} - \tau_s \langle |(\mathrm{d}/\mathrm{d}t)\, \delta_r \boldsymbol{u}|^2 \rangle^{1/2} \approx C\varepsilon^{1/3} r^{1/3} - \tau_s \langle |\delta_r \boldsymbol{a}|^2 \rangle^{1/2}, \tag{4.19}$$

where $\delta_r \boldsymbol{a} = \delta_r(\partial_t \boldsymbol{u} + \boldsymbol{u} \cdot \nabla \boldsymbol{u})$ denotes the increment of the fluid acceleration over the separation r. Next we assume scaling invariance of the turbulent acceleration field, that is, according to dimensional arguments of K41 theory, $|\delta_r \boldsymbol{a}| \sim \varepsilon^{2/3} r^{-1/3}$. Equation (4.19) can then be rewritten as

$$\dot{r} = C\varepsilon^{1/3} r^{1/3} \left(1 - A\, \tau_s\, \varepsilon^{1/3} r^{-2/3}\right) = C\varepsilon^{1/3} r^{1/3} \left(1 - A\, St(r)\right), \tag{4.20}$$

where A is an order-unity constant. The initial condition is given by $r(t_0) = r_0$ where the initial separation has to be chosen such such that $St(r_0) \ll 1$. We can next integrate the approximate dynamics perturbatively in terms of the small parameter $St(r_0)$ by expanding the separation as $r(t) = \rho_0(t) + \rho_1(t) + \rho_2(t) + \ldots$. The leading order is $\rho_0(t) = [r_0^{2/3} + (2C/3)\, \varepsilon^{1/3} t]^{3/2}$ and corresponds to the relative dispersion of a pair of tracers. The first-order correction reads $\rho_1(t) = -\tau_s\, \varepsilon^{1/3} A\, \ln(\rho_0(t)/r_0)\, \rho_0^{1/3}(t)$. At times much larger than the Batchelor time associated to the initial separation r_0, i.e. for $t \gg \varepsilon^{-1/3} r_0^{2/3}$, the leading term follows the Richardson explosive law $\rho_0(t) \simeq (2C/3)^{3/2} \varepsilon^{1/2} t^{3/2}$. This finally implies that in the asymptotics $t \gg \varepsilon^{-1/3} r_0^{2/3} \gg \tau_s$, one can write

$$r^2(t) \propto g\, t^3 \left[1 - D\, (t/\tau_s)^{-1} \ln (t/\tau_s)\right], \tag{4.21}$$

where g is the Richardson constant introduced in §4 and D is an order-unity factor, which a priori does not depend neither on the particle Stokes number, nor on the initial particles separation.

This behaviour is confirmed numerically as can be seen from Fig. 9 that gives the behaviours at large times of the ratio $Q(t)$ between the mean square separation of heavy particles and that of tracers as defined by (4.4). One can clearly see that data almost collapse on a line $\propto 1/t$ confirming the behaviour (4.21) predicted above. Only results from Run I are displayed here. The reason is that the very large time statistics of tracer dispersion in Run II is not as well statistically converged, leading to more noisy data. The qualitative picture is however very similar.

To conclude this section, let us stress that we have assumed above K41 scaling to hold

for the acceleration field (and thus for the pressure gradient). However it is well known that the scaling properties of pressure are still unclear: they might depend on the turbulent flow Reynolds number and/or on the type of flow (see, e.g., Gotoh & Fukayama 2001, Xu *et al.* 2007). As stated in Bec *et al.* 2007, rather than being dominated by K41 scaling, numerically estimated pressure increments of Run I ($Re_\lambda \simeq 200$) seem to be ruled by sweeping, so that $|\delta_r \boldsymbol{a}| \sim u_{\rm rms}\, \varepsilon^{1/3} r^{-2/3}$. One can easily check that this difference in scaling leads to a behaviour similar to (4.21), except that this time logarithmic corrections are absent, and that the non-dimensional constant D depends on the Reynolds number of the flow. The present numerical data do not allow to distinguish between these two possible behaviors.

5. Probability density function of inertial particle separation

We now discuss the shape of the probability density function for both light and heavy inertial particles. We focus on the time and scale behaviour of the non-stationary PDF

$$\mathcal{P}_{St,\beta}(R,t|R_0,t_0)\,, \tag{5.1}$$

defined as the probability to find a pair of inertial particles (St,β), with separation R at time t, given their initial separation R_0 at time t_0. The case of tracers ($St=0,\beta=1$) has been widely studied in the past, either experimentally, numerically and theoretically for two and three dimensional turbulent flows (see Richardson 1929, Batchelor 1952, Jullien *et al.* 1999, Boffetta & Sokolov 2002, Biferale *et al.* 2005, Bourgoin *et al.* 2006, Salazar & Collins 2009). Following the celebrated ideas of Richardson, phenomenological modelling in terms of a diffusion equation for the PDF of pair separation leads to the well-known non-Gaussian distribution,

$$\mathcal{P}_{St=0,\beta=1}(R,t) \propto \frac{R^2}{\left(\varepsilon^{1/3}t\right)^{9/2}}\, \exp\left[-\frac{A\,R^{2/3}}{\varepsilon^{1/3}\,t}\right], \tag{5.2}$$

which is valid for times within the inertial range $\tau_\eta \ll t \ll T_L$, and is obtained assuming a small enough initial separation and statistical homogeneity and isotropy of the three-dimensional turbulent flow. Here, A is a normalization constant. This prediction is based on the simple assumption that, for inertial range distances, tracers undergo a diffusion dynamics with an *effective*, self-similar, turbulent diffusivity $K(R) \propto R\,\delta_R u \sim \varepsilon^{1/3}\,R^{4/3}$. Moreover, it relies on the phenomenological assumption that tracers separate in a short-time correlated velocity field. Indeed, it is only if the latter is true, that the diffusion equation for the pair separation becomes exact (see Falkovich *et al.* 2001).

As mentioned before such a scenario may be strongly contaminated by particle inertia. The main modifications are expected to be due to the presence of small-scale caustics for small-to-large Stokes numbers, and to preferential concentration. Caustics make the small scale velocity field not differentiable and not self-similar, as if inertial particles were separating in a rough velocity field whose exponent were depending on distance. Preferential concentration, leading to inhomogeneous spatial distribution of particles, manifests itself as a sort of *effective compressibility* in the particle velocity field.

There exists a series of stochastic *toy models* for Lagrangian motion of particles in incompressible/compressible velocity fields, where the statistics of pair separation can be addressed analytically. Among these, the so-called Kraichnan ensemble models, where tracer particles move in a compressible, short-time correlated, homogeneous and isotropic velocity field, with Gaussian spatial correlations (we refer the reader to the review Falkovich *et al.* 2001 for a description of this model). It is useful for the sequel to recall two main results obtained for relative dispersion in a Kraichnan compressible flow.

We denote with $\wp$ the velocity field compressibility degree†, and with $0 \leq \xi < 2$ the scaling exponent of the two-point velocity correlation function at the scale r, in d-dimensions: $\langle [u_i(\boldsymbol{r}) - u_i(0)][u_j(\boldsymbol{r}) - u_j(0)] \rangle \sim G_1 r^{\xi} [(d - 1 + \xi - \wp\xi)\delta_{ij} + \xi(\wp\, d - 1) r_i r_j / r^2]$. For particles moving in such flows, it is possible to show that the pair separation PDF for tracer particles follows a Richardson-like behaviour:

$$\mathcal{P}_{\mu,\xi}(R,t) \propto \frac{R^{D_2-1}}{t^{(d-\mu)/(2-\xi)}} \exp\left[-A\frac{R^{2-\xi}}{t}\right]. \tag{5.3}$$

Here $\mu = \wp\xi(d+\xi)/(1+\wp\xi)$ and $D_2 = d - \mu$ is the correlation dimension, characterizing the fractal spatial distribution of particles.
A different distribution emerges when the $d-$dimensional Kraichan flow is differentiable, i.e. for $\xi = 2$; in such case, a log-normal PDF is expected:

$$\mathcal{P}_{\mu,\xi}(R,t|R_0,t_0) \propto \frac{1}{R} \exp\left[-\frac{(\log(R/R_0) - \lambda(t-t_0))^2}{2\Delta(t-t_0)}\right], \tag{5.4}$$

with $\Delta = 2G_1(d-1)(1+2\wp)$ and $\lambda = G_1(d-1)(d-4\wp)$. It is worth noticing that in the latter case, since the flow is differentiable, the large-time PDF depends on the initial data.

The problem of inertial particle separation in a real turbulent flow presents some similarities with the previous toy cases but also important differences.
First, the effective degree of compressibility — due to preferential concentration of inertial particles —, is properly defined only in the dissipative range of scales. For $r \ll \eta$, it is equal to the correlation dimension D_2 defined as $p(r) \sim r^{D_2}$, where $p(r)$ is the probability to find two particles at distance smaller than r, with $r \ll \eta$. As it has been numerically shown in Bec *et al.* 2007, Calzavarini *et al.* 2008 for three-dimensional turbulent flows, the correlation dimension depends only on the degree of inertia (St, β), while it does not seem to depend on the Reynolds number of the flow. For $r \gg \eta$, the effective degree of compressibility is no longer constant, but varies with the scale.
Second, the underlying velocity field exhibits spatial and temporal correlations that are much more complex than in a Gaussian short-correlated field. Such correlations lead to non-trivial overlaps between particle dynamics and the carrying flow topology. As a result, it is not possible to simply translate the analytical findings obtained in the compressible Kraichnan ensemble to the case of inertial particles: we may expect however that in some limits the compressible Kraichnan results should give the leading behaviour also for the case studied here of inertial particles in real turbulent flows.

With this purpose, we first notice that the separation probability density function that is valid in the rough case (5.3) has an asymptotic stretched-exponential decay that is independent on the compressibility degree. This suggests that inertial particle PDF (5.1) must recover the Richardson behaviour (5.2) of tracers in the limit of large scales and large times. Coherently with what discussed in previous sections, for large times and for scales larger than R^*_{St}, we expect that the heavy pairs (in the limit $\beta \sim 0$) PDF recovers a tracer like distribution :

$$\mathcal{P}_{St,0}(R,t) \sim \exp\left[-A\frac{R^{2/3}}{\varepsilon^{1/3}t}\right]; \qquad R \gg R^*_{St}. \tag{5.5}$$

For pairs of light particles, there is no straightforward formulation of such a prediction:

† The compressibility degree $\wp$ is defined as the ratio $\wp \equiv \mathcal{C}^2/\mathcal{S}^2$, where $\mathcal{C}^2 \propto \langle (\nabla \cdot \boldsymbol{u})^2 \rangle$ and $\mathcal{S}^2 \propto \langle (\nabla \boldsymbol{u})^2 \rangle$, and varies between $\wp = 0$ for incompressible flows, and $\wp = 1$ for potential flows.

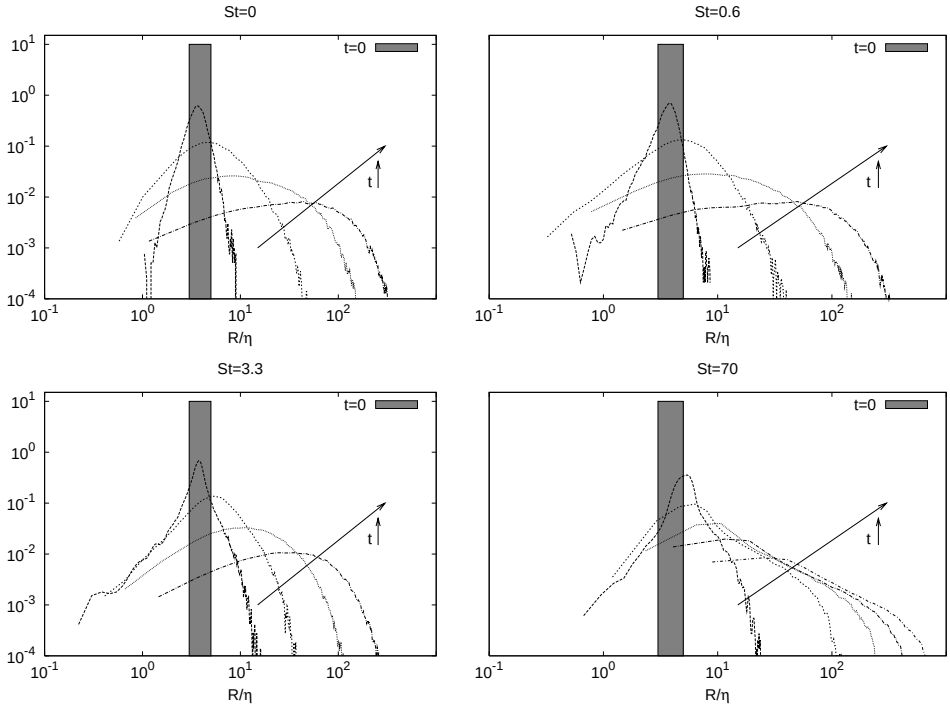

FIGURE 10. Separation probability density function, $\mathcal{P}(R,t|R_0,t_0)$, for heavy pairs with different Stokes numbers, at changing time. Initial distance is taken $R_0 \in [3:4]\,\eta$ for $St = 0$ (top-left), $St = 0.6$ (top-right), and $St = 3.3$ (bottom-left) of Run I, and equal to $R_0 \in [4:6]\,\eta$ for $St = 70$ (bottom-right) of Run II. The related initial distributions are pictorically depicted with a grey area. Times shown are: $(t-t_0)/\tau_\eta = 1, 6, 18, 36$ for Run I and $(t-t_0)/\tau_\eta = 1, 6, 18, 36, 86$ for Run II.

as we shall see in the sequel, preferential concentration effects have a strong fingerprint on the separation PDF even at large times and large scales.

In the opposite limit of very small separations, i.e. $R \ll \eta$, one can correctly assume that the effective degree of compressibility is constant and therefore apply either the small-scale limit for rough flows (5.3), or that for smooth flows (5.4), depending on the scaling properties of the particle velocity field entailed in the value of the exponent $\gamma(St)$, defined from (3.4) and related to the caustics. We thus expect

$$\begin{aligned} &\mathcal{P}_{St,\beta}(R,t|R_0,t_0) \sim R^{\frac{D_2}{2}-1} G(t), \qquad \text{if } \gamma(St) \neq 1, \\ &\mathcal{P}_{St,\beta}(R,t|R_0,t_0) \sim R^{D_2-1} F(t), \qquad \text{if } \gamma(St) = 1. \end{aligned} \tag{5.6}$$

Here F and G are two different decaying functions of time t, whose expression can be easily derived from (5.3)-(5.4). Notice that for the smooth case, i.e. the small-scale limit of the log-normal distribution (5.4), we get for the spatial dependency a factor $D_2/2$ instead of the factor D_2 of the rough case. This will matter in the case of light particle separation, where, due to strong preferential concentration, the probability of finding pairs at a very small distances is large enough to allow for a detailed test of the prediction (5.6). The case of light particles will be discussed in §6, while we now turn to a discussion of the above scenario in the case of heavy particle pairs.

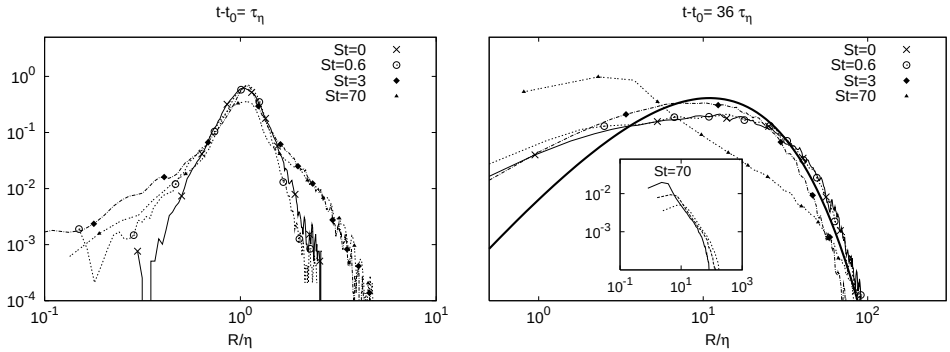

FIGURE 11. Comparison of PDFs at fixed times with data of Fig.(10). Left: early stage of the separation process, $t - t_0 = \tau_\eta$. Inertia does not affect small Stokes, $St = 0.6$ while its effect is detectable for $St = 3$ and $St = 70$. Right: PDFs comparison at a later time, $t - t_0 = 36\tau_\eta$. Now the PDF shows some deviations from the tracer behaviour only for $St = 70$. On the right panel the solid line gives the Richardson shape (5.2). Initial separation and Reynolds numbers are the same as for Fig. (10). The inset shows the PDF evolution for $St = 70$ at three times, $(t - t_0)/\tau_\eta = 36, 82, 130$.

5.1. *Probability density function of heavy particle relative separation*

We start by analyzing the qualitative evolution of $\mathcal{P}_{St}(R, t)$ at changing time, for different Stokes numbers and in the limit $\beta = 0$. The four panels of Fig. 10 show the evolution of the PDF at different times for pairs with $St = 0$ (tracers), and for heavy particles with $St = 1$, 3.3, and 70. Initially, at $t = t_0$, all selected pairs are separated by the same distance ($R_0 \in [3\!:\!6]\,\eta$); this initial distribution is represented in each figure by a grey area. As time elapses, particle separate and reach different scales, depending on their inertia. Qualitatively, the PDF evolution is very similar for all moderate Stokes numbers, and the PDFs at different moderate Stokes numbers become more and more similar with time. However in the case of $St = 70$ — for which the associate Stokes time τ_s falls well inside the inertial range — , the PDF shows a long exponential tail for intermediate separation, which tends to persist at all observed times. To better appreciate such differences, in Fig. 11 we show the comparison between the different PDFs corresponding to various Stokes numbers for two different times: at the beginning of the separation process, $(t - t_0) = \tau_\eta$, and at a later time, $(t - t_0) = 36\tau_\eta$. As one can see, it is only at early times that the PDFs for moderate-to-large Stokes, $St = 3, 70$ differ in a sensible way from the tracers. In particular, one can clearly see that many pairs have separations much larger and much smaller than those observed for tracers or for heavy pairs with small Stokes numbers. The right tails, describing pairs that are very far apart, are just the signature of the *scrambling* effect of caustics. Such strong events are not captured by second order moments of the separation statistics that we discussed before, while they clearly affect higher-order moments. The left tails, associated to pairs much closer than tracers, are possibly due to particles that separate at a slower rate than tracers because of preferential concentration induced by inertia.

Later in the evolution, for $(t - t_0) = 36\tau_\eta$, only the separation PDF for $St = 70$ still shows important departure from the tracer case; for all the other Stokes numbers shown, pairs have had enough time to forget their initial distribution and have practically relaxed on the typical Richardson-like distribution. In the inset, we also show the persistence in the exponential behaviour for the PDF at $St = 70$, by superposing the shapes measured at three times during the particles separation.

With the present data the small scale asymptotic behaviour (5.6) cannot be validated

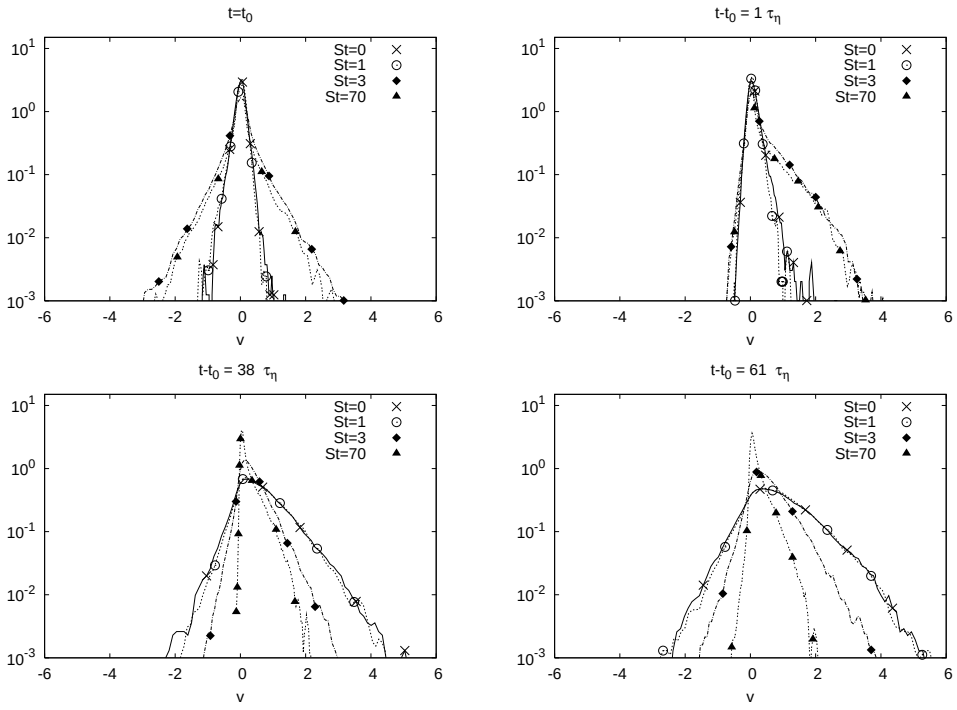

FIGURE 12. Time evolution of the probability density function of heavy particle relative longitudinal velocity, $\mathcal{W}_{St}(v,t)$, during the separation process. Data refers to four different cases: tracers pairs $St = 0$, and heavy pairs $St = 1, 3, 70$, starting with initial distance $R_0 \in [4:6]\eta$. PDFs are measured at times $(t - t_0) = [0, 1, 38, 61]\tau_\eta$, for Run II. Notice the presence of intense velocity fluctuations for moderate-to-strong inertia, $St = 3, 70$, observable at the early stage of the separation process. These are the legacy of the caustics distribution.

for heavy particles. This is due to the limited statistics: very soon after the initial time t_0, there are almost no pairs left with separations $R \ll \eta$.

5.2. *Probability density function of heavy particle relative velocities*

At moderate to large Stokes numbers the separation process of heavy particle pairs is largely influenced by the presence of large velocity differences at small scales, that is by the presence of caustics in the particles velocity field. In §3, we have studied stationary statistics (only first-order moment) of velocity differences between heavy particles at changing the distance between particles and their inertia. However it is also informative to look at the non-stationary, time-dependent distribution of velocity differences, and more particularly to its distribution measured along heavy pairs separation. The relative velocity $\delta_R \boldsymbol{V}(t) = \dot{\boldsymbol{X}}_1(t) - \dot{\boldsymbol{X}}_2(t)$ can be decomposed into the projection along the separation vector, and two transveral components, here equivalent since the system is statistically isotropic. For tracer particles, the statistics of relative velocity and the alignment properties of $\delta_R \boldsymbol{V}(t)$ and $\boldsymbol{R}(t)$ have been discussed extensively (see e.g. Yeung & Borgas 2004). Here, we focus on the PDF of the relative longitudinal velocity only, which we denote by $\mathcal{W}_{St}(v,t)$, where $v(t) = [\dot{\boldsymbol{X}}_1(t) - \dot{\boldsymbol{X}}_2(t)] \cdot \hat{\boldsymbol{R}}(t)$. For pairs of tracers ($St = 0$), the initial longitudinal velocity distribution is nothing else than the PDF of Eulerian longitudinal velocity increments measured at the distance R_0. For pairs of inertial particles, this initial PDF clearly coincides with the stationary distribution of velocity differences between particles that are at a distance $R = |\boldsymbol{X}_1(t_0) - \boldsymbol{X}_2(t_0)| \in [R_0 : R_0 + dR_0]$. Such a distribu-

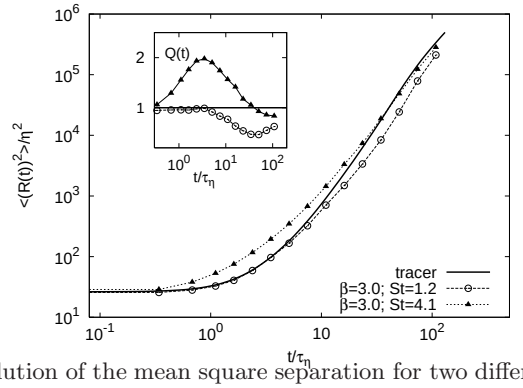

FIGURE 13. Time evolution of the mean square separation for two different families of light particles ($St = 1.2, \beta = 3$) and ($St = 4.1, \beta = 3$). The case of tracers is also shown for comparison. Notice that the strong small-scale clustering does not affect the long-time behaviour, except through a very small asymptotic slow down. Inset: ratio between the mean square separation for light pairs and that of tracers.

tion has the signature of two mechanisms: (i) at small Stokes numbers, only preferential concentration matters and particles probe only a sub-set of all possible fluid velocity fluctuations; (ii) at large Stokes numbers, particles are homogeneously distributed but with a velocity field which may be strongly different from the underlying fluid velocity.

For what concerns heavy pairs, the first effect has not an important signature on small-scale quantities. However the second effect clearly becomes visible for moderate to high inertia as shown in Fig. 12. Here we report the longitudinal velocity distributions for pairs with initial distance $R_0 \in [4:6]\,\eta$, and with $St = 0, 1, 3.3$, and 70; the Reynolds number of the underlying flow is $Re_\lambda \sim 400$. Each panel contains the PDFs measured at different times spanning all turbulent timescales. At $t = t_0$, the importance of caustics is manifest for the two largest Stokes numbers, leading to fat tails towards both small and large velocity differences. Interestingly enough, the left tail of $\mathcal{W}_{St}(v,t)$, which describes approaching events of particle relative motion, is immediately dumped already at $(t - t_0) \sim \tau_\eta$; at the same time, however, the right tail continues to be quite fat for the two largest Stokes numbers under consideration. At later stages of the separation process, the tendency of large-Stokes-number pairs to wash out approaching events becomes even stronger. Indeed, at time $(t - t_0) = 38\,\tau_\eta$, the small velocity increments tail has almost disappeared for pairs with $St = 70$. It is worth noticing that at those times (i.e. also at those typical scales), heavy particle velocity differences have already started to be smaller than the tracer velocity increments: the larger is the Stokes number, the less pronounced are the PDF tails.

Summarising, because of the different effects of inertia, we observe a very complex evolution for the longitudinal relative velocity fluctuations along the trajectories of heavy particle pairs. This is certainly a key issue to be considered for stochastic modelling: here, as in a standard *kinetic* problem, both particle positions and velocities need to be modelled to quantitatively control the relative dispersion process.

6. Relative dispersion for light particles

So far we have considered the relative motion of very heavy particle pairs, for which the density contrast β with the underlying fluid is zero. In this section we present results on light particles dynamics as described by (2.2), for different possible choices of the parameters (St, β).

We discuss how the strong effect of preferential concentration — typically observed in

the case of light particles in turbulent flows — might influence the intermediate and long-time behaviour of pair separations. In three-dimensional turbulent flows, as we consider here, light particles associated to different values of (St, β) have been observed to always possess a positive largest Lyapunov exponent Calzavarini *et al.* 2008: this implies that light pairs always separate in $3d$ real turbulent flows. We recall, however, that this is not always true: for instance, in smooth two-dimensional random flows, there are values of (St, β) for which the largest Lyapunov exponent can become negative and particles form pointwise clusters (see Bec 2003).

Light particles with moderate inertia and high density ratio (order-unity St, and $\beta = 3$), initially tend to separate much slower than heavy particles with the similar Stokes number: this is evident from the much smaller values of the Lyapunov exponents measured for light particles, with respect to those measured for heavy particles with equivalent Stokes numbers but $\beta = 0$. Moreover, finite-time Lyapunov exponents show large fluctuations, indicating that there are pairs that do not separate even at long times. Results on this issue will be reported elsewhere. Clearly, pairs of light particles that do not separate do not influence the mean square distances: hence, we do not expect, and indeed do not measure, any large differences for the long-time behaviour of $\langle |\boldsymbol{R}(t)|^2 \rangle_{St,\beta}$ for light particles, with respect to the heavy case (see Fig. 13).

It is natural to ask if light particle strong preferential concentration affects high-order moments of relative separation of two initially close particles, and particularly the left tail of the separation PDF. Figure 14 shows the time evolution of the separation probability density function, $\mathcal{P}_{St,\beta}(R, t|R_0, t_0)$. Data refer to a case with very intense preferential concentration effects and minor influence of caustics ($St = 1.2, \beta = 3$), and a case with milder inhomogeneities in the spatial distribution ($St = 0.3, \beta = 2$). The initial separation PDF was chosen in both cases by selecting particle pairs with initial distance $R_0 \in [4:6]\,\eta$. A remarkable observation is a strong tendency to fill small separations. In other words there are many pairs that reduce their mutual distance even for a very long times. The development of the left tail for the strong clustering case ($St = 1.2, \beta = 3$) is consistent with the estimate given by the long-time, small-scale asymptotic expansion of the log-normal distribution (5.6), $\mathcal{P}(R, t) \sim R^{D_2/2-1}$, as shown by the straight line in the plot. This is the confirmation that the small-scale dynamics of the highly clustered light particles evolves as that of tracers moving in a smooth, compressible flow (characterised by the same D_2).

We also remark that if there is high spatial preferential concentration, caustics cannot be important. This may have important consequences for the estimation of collision kernel of light particles. The approaching events, shown by the left tail in Figure 14, are clearly due to the preferential concentration inside vortex-like structures, typical of light particles. The right panel show a different case, where preferential concentration is less important, leading to a correlation dimension $D_2 = 2$. Of course, also in this latter case, there are events with approaching pairs, but these become less and less probable with time.

The importance of preferential concentration can also be appreciated by looking at the PDFs of longitudinal velocity differences between light particles during the separation. We show such distributions for one of the pair family considered above, and we compare them with those of the tracers (see Fig. 15). The important difference between the two cases stems from the highly peaked nature of the relative velocity PDF for the strong clustered light particle case. The presence of many pairs with almost vanishing velocity differences is the signature of a coherent bunch of pairs moving on a strongly clustered set.

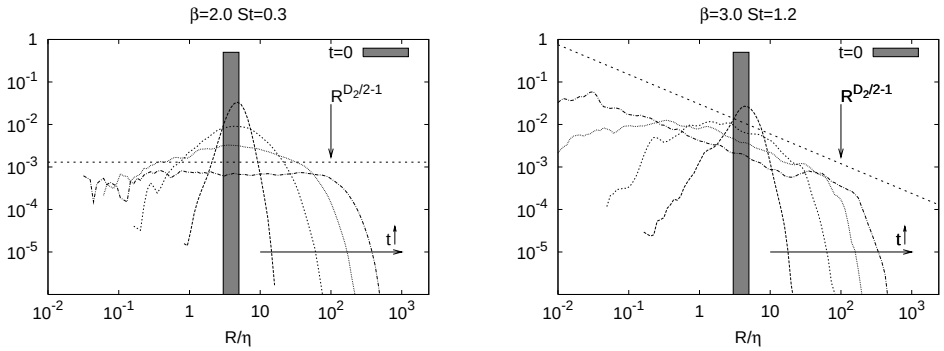

FIGURE 14. Time evolution of the separation probability density functions of light particles. Left panel: $St = 0.3, \beta = 2$, corresponding to a case where preferential concentration is not very effective ($D_2 = 2$). As time elapses, one observes a self-similar filling toward smaller separations, in agreement with (5.6) (dashed line). Right panel: $St = 1.2, \beta = 3$, corresponding to light particles with strong clustering properties (correlation dimension $D_2 = 0.8$). Again the self-similar filling of small scales is consistent with the prediction $D_2/2 - 1$ as depicted by the dashed straight line.

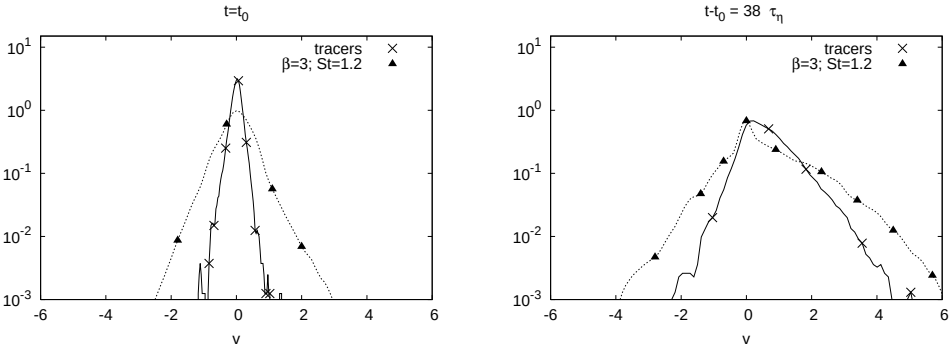

FIGURE 15. Probability density functions of relative longitudinal velocity, $\mathcal{W}_{St,\beta}(v,t)$, for light pairs with $St = 1.2, \beta = 3$, and for tracers ($St = 0, \beta = 1$). PDFs are measured along the separation process at two different times: left panel refers to the initial time, $t = t_0$; while right panel refers to $t - t_0 = 38\tau_\eta$.

7. Conclusions

We have studied the relative dispersion of inertial particles in homogeneous and isotropic turbulence from two DNS at resolutions 512^3 and 2048^3, corresponding to $Re_\lambda \sim 200$ and $Re_\lambda \sim 400$, respectively. We have analysed both heavy and light particle statistics at changing the Stokes numbers. We have studied the evolution of mean separations and the whole PDFs' shape, both for particle distance and velocity increments at changing time and for different typical initial distances. The main results that we have discussed can be summarised as follows. Separations of very heavy particles, with Stokes times falling in the inertial range of the underlying fluid, are strongly affected by the presence of caustics up to times, when the distance between particles reaches scales that are large enough for the separation dynamics to be again dominated by the underlying flow velocity. As a consequence, strong transient departure from the Richardson diffusion, with a faster ballistic regime, is observed. A statistical closure of the equation of motions for heavy particle separation is also developed. This model is able to reproduce the main numerical findings.

For light particles, at high density ratio, we observe strong small-scale clustering prop-

erties, leading to a considerable fraction of pairs that do not separate at all — although the maximum Lyapunov exponent remains positive. In such a case, the non-stationary spatial concentration at small scales tends to be higher than the analogous case but with a stationary distribution of particles. Such numerical findings open the way to experimental verifications and gives input to the community involved in modelling inertial particle diffusion in applied configurations.

We thank Massimo Cencini, who collaborated at an early stage of this work, for very fruitful and continuous exchange of ideas. This study benefitted from constructive discussions with E. Bodenschatz, E. Calzavarini, L. Collins and G. Falkovich to whom we wish to express a warm gratitude. J. Bec and A.S. Lanotte aknowledge support from the National Science Foundation under grant No. PHY05_51164 for their stay at the Kavli Institute for Theoretical Physics in the framework of the 2008 "Physics of the Climate Change" program. Part of this work was supported by Agence Nationale de la Recherche under grant No. BLAN07-1_192604. We thank the DEISA Consortium (co-funded by the EU, FP6 project 508830), for support for Run II within the DEISA Extreme Computing Initiative (www.deisa.org). Numerical simulations of Run I were performed at CASPUR (Italy) and CINECA (Italy). Numerical raw data of particle trajectories are freely available from the iCFDdatabase (http://cfd.cineca.it) kindly hosted by CINECA (Italy).

REFERENCES

Ayyalasomayajula, S., Warhaft, Z. & Collins, L.R. 2008 Modeling inertial particle acceleration statistics in isotropic turbulence. *Phys. Fluids* **20** 095104.

Balkovsky, E., Falkovich, G. & Fouxon, A. 2001 Intermittent distribution of inertial particles in turbulent flows. *Phys. Rev. Lett.* **86**, 2790–2793.

Batchelor, G.K. 1952 Diffusion in a field of homogeneous turbulence II. The relative motion of particles. *Proc. Camb. Philos. Soc.* **48**, 345–362.

Bec, J. 2003 Fractal clustering of inertial particles in random flows *Phys. Fluids* **15**, L81–L84.

Bec, J., Celani, A., Cencini, M. & Musacchio, S. 2005 Clustering and collisions of heavy particles in random smooth flows. *Phys. Fluids* **17**, 073301.

Bec, J., Biferale, L., Boffetta, G., Celani, A., Cencini, M., Lanotte, A.S., Musacchio, S., & Toschi, F. 2006 Acceleration statistics of heavy particles in turbulence. *J. Fluid Mech.* **550**, 349–358.

Bec, J., Biferale, L., Boffetta, G., Cencini, M., Lanotte, A.S., Musacchio, S. & Toschi, F. 2007 Heavy particle concentration in turbulence at dissipative and inertial scales. *Phys. Rev. Lett.* **98**, 084502.

Bec, J., Cencini, M., Hillerbrand, R. & Turitsyn, K. 2008 Stochastic suspensions of heavy particles *Physica* D **237**, 2037–2050.

Biferale, L., Boffetta, G., Celani, A., Devenish, B.J., Lanotte, A.S. & Toschi, F. 2005 Lagrangian statistics of particle pairs in homogeneous isotropic turbulence. *Phys. Fluids* **17**, 115101.

Biferale L., Boffetta, G., Celani, A., Lanotte, A.S. & Toschi, F. 2005 Lagrangian statistics of fully developed turbulence. *J. Turb.* **7**, 6(1-12).

Boffetta, G. & Sokolov, M. 2002 Statistics of two-particle dispersion in two-dimensional turbulence. *Phys. Fluids* **14**, 3224–3232.

Boffetta, G., De Lillo, F. & Gamba, A. 2004 Large scale inhomogeneity of inertial particles in turbulent flows. *Phys. Fluids* **16**, L20–L24.

Boivin, M., Simonin, O. & Squires, K.D. 1998 Direct numerical simulation of turbulence modulation by particles in isotropic turbulence. *J. Fluid Mech.* **375**, 235–263.

Bourgoin, M., Ouelette, N.T., Xu, H., Berg, J. & Bodenschatz, E. 2006 The role of pair dispersion in turbulent flow. *Science* **311** 835–838.

Calzavarini, E., Kerscher, M., Lohse, D. & Toschi, F. 2008 Dimensionality and morphology of particle and bubble clusters in turbulent flow. *J. Fluid Mech.* **607**, 13–24.

Cencini, M., Bec, J., Biferale, L., Boffetta, G., Celani, A., Lanotte, A.S., Musacchio, S. & Toschi, F. 2006 Dynamics and statistics of heavy particles in turbulent flows. *J. Turb.* **7**, 36, 1.

Chen, S., Doolen, G.D., Kraichnan, R.H. & She, Z.-S. 1993 On statistical correlations between velocity increments and locally averaged dissipation in homogeneous turbulence. *Phys. Fluids A* **5**, 458–463.

Chun, J., Koch, D.L., Rani, S., Ahluwalia, A. & Collins, L.R. 2005 Clustering of aerosol particles in isotropic turbulence. *J. Fluid Mech.* **536**, 219–251.

Collins, L.R. & Keswani, A. 2004 Reynolds number scaling of particle clustering in turbulent aerosols. *New J. Phys.* **6**, 119.

Csanady, G. 1980 *Turbulent diffusion in the environment.* Geophysics and Astrophysics Monographs Vol. 3 D. Reidel Publishing Company.

Derevich, I.V. 2008 Relative particle velocity in a turbulent flow. *Fluid Dyn.* **43**, 357–368.

Douady, S., Couder, Y. & Brachet, M.-E. 1991 Direct observation of the intermittency of intense vorticity filaments in turbulence. *Phys. Rev. Lett.* **67**, 983–986.

E, W. & Vanden Eijnden, E. 2000 Generalized flows, intrinsic stochasticity, and turbulent transport. *Proc. Nat. Acad. Sci. (USA)* **97**, 8200–8205.

Eaton, J.K.& Fessler, J.L. 1994 Preferential concentrations of particles by turbulence. *Intl. J. Multiphase Flow* **20**, 169–209.

Falkovich, G., Gawędzki, K. & Vergassola, M. 2001 Particles and fields in fluid turbulence. *Rev. Mod. Phys.* **73**, 913–975.

Falkovich, G., Fouxon, A. & Stepanov, M. 2002 Acceleration of rain initiation by cloud turbulence. *Nature* **419**, 151–154.

Falkovich, G. & Pumir, A. 2004 Intermittent distribution of heavy particles in a turbulent flow. *Phys. Fluids* **16**, L47–L51.

Falkovich, G. & Pumir, A. 2007 Sling effect in collision of water droplet in turbulent clouds. *J. Atm. Sci.* **64**, 4497–4505.

Fouxon, I. & Horvai, P. 2008 Separation of heavy particles in turbulence. *Phys. Rev. Lett.* **100** 040601.

Frisch, U. 1995 *Turbulence. The legacy of A.N. Kolmogorov* Cambridge University Press, Cambridge (UK).

Gerashchenko, S., Sharp, N.S., Neuscamman, S. & Warhaft, Z. 2008 Lagrangian measurements of inertial particle accelerations in a turbulent boundary layer. *J. Fluid Mech.* **617**, 255–281.

Goto, S. & Vassilicos, J.C. 2008 Sweep-stick mechanism of heavy particle clustering in fluid turbulence. *Phys. Rev. Lett.* **100** 054503.

Gotoh, T. & Fukayama, D. 2001 Pressure spectrum in homogeneous turbulence. *Phys. Rev. Lett.* **86**, 3775–3778.

Gylfason, A., Ayyalasomayajula, S., Bodenschatz, E. & Warhaft, Z. 2006 Lagrangian measurements of inertial particle accelerations in grid generated wind tunnel turbulence. *Phys. Rev. Lett* **97**, 144507.

Jullien, M.-C., Paret, J. & Tabeling, P. 1999 Richardson pair dispersion in two-dimensional turbulence. *Phys. Rev. Lett.* **82**, 2872–2876.

Maxey, M.R. & Riley, J. 1983 Equation of motion of a small rigid sphere in a nonuniform flow. *Phys. Fluids* **26**, 883–889.

Maxey, M.R. 1987 The motion of small spherical particles in a cellular flow field. *Phys. Fluids* **30**, 1915–1928.

Mehlig, B. & Wikinson, M. 2004 Coagulation by random velocity fields as a Kramers problem. *Phys. Rev. Lett.* **92**, 250602.

Meneveau, C. 1996 Transition between viscous and inertial-range scaling of turbulence structure functions 1996 *Phys. Rev.* E **54**, 3657–3663.

Monin, A.S. & Yaglom, A.M. 2007 *Statistical Fluid Mechanics, Volume 2: Mechanics of Turbulence* Cambridge, MA/London, UK.: MIT. 874 pp.

Olla, P. 2002 Transport properties of heavy particles in high Reynolds number turbulence. *Phys. Fluids* **14**, 4266–4277.

Ott, S. & Mann, J. 2000 An experimental investigation of the relative di usion of particle pairs in three-dimensional turbulent flow. *J. Fluid Mech.* **422**, 207–223.

Ouellette, N.T., Xu, H., Bourgoin, M. & Bodenschatz, E. 2006 An experimental study of turbulent relative dispersion models. *New J. Phys.* **8**, 109 (1–22).

Post, S. & Abraham, J. 2002 Modeling the outcome of drop-drop collisions in Diesel sprays. *Intl. J. Multiphase Flow* **28**, 997–1019.

Qureshi, N.M., Bourgoin, M., Baudet, C., Cartellier, A., & Gagne, Y., 2007 Turbulent transport of material particles: An experimental study of finite size effects. *Phys. Rev. Lett* **99**, 184502.

Reade, W.C. & Collins, L.R. 2000 A numerical study of the particle size distribution of an aerosol undergoing turbulent coagulation. *J. Fluid Mech.* **415**, 45–64.

Richardson, L.F. 1929 A search for the law of atmospheric diffusion. *Beitr. Phys. Frei. Atmos.* **15**, 24–29.

Salazar, J.P.L.C. & Collins, L.R. 2009 Two-particle dispersion in isotropic turbulent flows. *Ann. Rev. Fluid Mech* **41** 405–432.

Sawford, B. 2001 Turbulent relative dispersion. 2001 *Ann. Rev. Fluid Mech.* **33**, 289–317.

Shaw, R.A. 2003 Particle-turbulence interactions in atmospheric clouds. *Ann. Rev. Fluid Mech.* **35**, 183–227.

Sigurgeirsson H. & Stuart A.M. 2002 A Model for Preferential Concentration. *Phys. Fluids* **14**, 4352–4361.

Squires, K.D. & Eaton, J.K. 1991 Preferential concentration of particles by turbulence. *Phys. Fluids A* **3**, 1169–1178.

Toschi, F. & Bodenschatz, E. 2009 Lagrangian Properties of Particles in Turbulence. *Ann. Rev. Fluid Mech.* **41**, 375–404 .

Volk, R., Mordant, N., Verhille, G. & Pinton, J.-F. 2008 Laser Doppler measurement of inertial particle and bubble accelerations in turbulence, *Europhys. Lett* **81**, 34002.

Wilkinson M. & Mehlig B. 2005 Caustics in turbulent aerosols. *Europhys. Lett* **71**, 186–192.

Xu, H., Ouellette, N.T., Vincenzi, D. & Bodenschatz, E. 2007 Acceleration correlations and pressure structure functions in high-Reynolds number turbulence. *Phys. Rev. Lett.* **99**, 204501.

Xu H. & Bodenschatz E. 2008 Motion of inertial particles with size larger than Kolmogorov scale in turbulent flows. *Physica* D **237**, 2095–2100.

Yeung P.K. & Borgas M.S. 2004 Relative dispersion in isotropic turbulence: Part 1. Direct numerical simulations and Reynolds number dependence. *J. Fluid Mech.* **503**, 125–160.

Zaichik, L.I., Simonin, O. & Alipchenkov, V.M. 2003 Two statistical models for predicting collision rates of inertial particles in homogeneous isotropic turbulence. *Phys. Fluids* **15**, 2995–3005.

Zaichik, L.I. & Alipchenkov, V.M. 2008 Acceleration of heavy particles in isotropic turbulence. *Intl. J. Multiphase Flow* **34**, 865–868.